Development and Evaluation of Contrail Models

by

Michael Xu

B.S. Mechanical Engineering, University of Illinois at Urbana-Champaign (2021)

Submitted to the Department of Aeronautics and Astronautics in Partial Fulfillment of the

Requirements for the Degree of

Master of Science in Aeronautics and Astronautics

at the

Massachusetts Institute of Technology

May 17, 2024

Authored by: Michael Xu

                Department of Aeronautics and Astronautics

                May 2024

Certified by: Steven R.H. Barrett

                H.N. Slater Professor of Aeronautics and Astronautics

                Thesis Supervisor

Certified by: Sebastian D. Eastham

                Visiting Associate Professor of Aeronautics and Astronautics

                Thesis Supervisor

Accepted by: Jonathan P. How

                R.C. Maclaurin Professor of Aeronautics and Astronautics

                Chair, Graduate Program Committee

Development and Evaluation of Contrail Models

by

Michael Xu

Submitted to the Department of Aeronautics and Astronautics on May 17, 2024 in Partial Fulfillment of the Requirements for the Degree of Master of Science in Aeronautics and Astronautics

Abstract

Condensation trails (contrails) are aircraft-induced ice clouds that are estimated to account for up to 50% of aviation's climate impacts. Uncertainties in the impact of individual contrails have motivated the development of contrail models, such as CoCiP, a 0-D rapid assessment model, and APCEMM, a 2-D model with detailed ice microphysics.

However, there are gaps within the current contrail modeling literature. There is no model both sufficiently fast for rapid assessment of contrail impacts and detailed in its ice microphysics modeling. There are few studies calibrating and validating the performance of contrail models on individual flights. The absolute and relative magnitudes of errors due to weather data uncertainty and errors due to modeling assumptions have not been extensively studied, despite many studies relying on the CoCiP model and the ERA5 weather data for their analyses.

This thesis addresses these gaps. The APCEMM model is optimized to achieve a decrease in runtime by 95% and is improved with depth estimation, vertical advection, and atmospheric turbulence modules. A set of 152 flight-attributed LIDAR cross sections is assembled to compare APCEMM and CoCiP results against individual contrail observations on metrics such as contrail width, depth, and optical depth. A method dubbed "ambient parameter inference", where contrail models infer the meteorological conditions necessary to reproduce a contrail observation, is developed to produce estimated distributions of ambient parameters. These distributions are used to analyze model sensitivities, biases in the weather data, and errors due to weather data uncertainty and modeling assumptions.

I find that the distributions of the wind shear and vertical humidity profile as inferred by APCEMM have means and medians within the range of radiosonde measurements of these quantities, suggesting that the model adequately accounts for the sensitivities of contrail properties to these parameters. Compared to the APCEMM-inferred parameters, the ERA5 weather data predicts a 3.8 times higher average supersaturated layer depth and a 56% lower wind shear, suggesting systematic biases.

CoCiP infers on average a 39% lower supersaturated layer depth and a 3.0 times higher ice supersaturation level compared to APCEMM. Due to the APCEMM-inferred parameters' closer agreement with radiosonde measurements, this suggests that there may be modeling errors due to CoCiP's inability to resolve the contrail's vertical profile and its lower sensitivity to relative humidity. Errors in the ambient humidity data are found to possibly account for an over 100% average absolute error in optical depth when using APCEMM, greater than the 72.5% attributable to CoCiP modeling limitations. APCEMM is found to predict contrails with a 29.3% longer average lifetime and a 4.34-5.92 times average higher energy forcing compared to CoCiP when using the ERA5 weather data. This suggests that inter-model disagreement is on the same order of magnitude as the already known errors resulting from meteorological data gaps.

Thesis Supervisor: Steven R.H. Barrett
Title: H.N. Slater Professor of Aeronautics and Astronautics

Thesis Supervisor: Sebastian D. Eastham
Title: Visiting Associate Professor of Aeronautics and Astronautics

Acknowledgements

I would like to express my sincere gratitude towards everyone who helped me through my journey. It's been a really eventful, humbling, and incredible two years for me. First, I would like to thank my advisor Sebastian Eastham for walking me through the process of diving into a topic I knew nothing about, helping me finding areas to push my research towards, and the incredible ideas generated in our fruitful technical discussions. I would also like to thank Steven Barrett for providing me the opportunity to perform this exciting research and for the academic and professional support. I would like to thank all my fellow students at LAE for creating such a supportive and collaborative work environment that made me thoroughly enjoy my time here. A special shout out to Vincent for the help with the LIDAR cross section data and the insightful feedback on my conference posters. This work would not be where it is without you. To my best friend, thank you Nasu. You're always there to make me laugh, and my life would not be the same without you. Yarimasune! Finally, Mom, thank you. You're always so proud and supportive of me regardless the dumb, spontaneous things I choose to do at any given moment despite 7000 miles away, and I would not be where I am without your unwavering support.

Contents

List of Figures

List of Tables

1 Introduction

Condensation trails (contrails) are line-shaped ice clouds that form behind aircraft at cruising altitudes through mixing of the engine exhaust and ambient air. They are estimated to account for 51% of aviation's current effective radiative forcing (RF), a measure of climate impact [1]. Although the overall RF of contrails as a whole is positive, individual contrails can be either warming or cooling, and their RF contributions can vary by several orders of magnitude. Factors that affect an individual contrail's climate impact include the ambient meteorological conditions and the aircraft engine emissions.

The variance in the RF of individual contrails motivates the development of models that predict the formation, evolution, and impacts of contrails. Two such models are the Contrail Cirrus Prediction Tool (CoCiP) [2] and the Aircraft Plume Chemistry, Emissions, and Microphysics Model (APCEMM)[3]. CoCiP is commonly used in studies evaluating contrail climate impacts [4] [5], is fast to run, and implementations such as pycontrails [6] make the model easy to get started with. The speed, however, comes with the disadvantage that it relies on single-equation parameterizations for the ice physics that govern the properties and impact of the contrail. Additionally, it does not simulate the contrail on a spatial grid and assumes that the contrail takes the shape of an ellipse, while observations and high-fidelity simulations of contrails reveal more complex shapes [7]. Despite these limitations of CoCiP, few attempts have been made to quantify the errors arising from these modeling simplifications that these contrail impact studies base their results on.

The second model, APCEMM, explicitly simulates the contrail physics and was developed to serve as a higher fidelity option for simulating contrail climate impacts. It uses a 2-D grid to simulate the contrail cross section, and represents the ice crystal size distribution using a binned scheme with detailed ice microphysics. However, APCEMM has many limitations. It uses unphysical periodic boundary conditions to accommodate a spectral solver [8] that requires artificial diffusion to stabilize, takes on the order of 2-10 hours to finish a contrail simulation compared to runtimes on the order of 10 seconds to 1 minute for CoCiP, and fails to capture important physical phenomena that

9

impact contrail behavior such as updrafts and atmospheric turbulence [9]. In addition, it assumes a constant aspect ratio for the initial contrail plume, while CoCiP has a more informed estimate of the initial width and depth. The contrail depth in particular is important because errors in its estimation will propagate to errors in other key contrail properties correlated with RF impact, such as width and optical depth [9]. Without addressing these problems with APCEMM, it is not easily used for large-scale evaluations of contrail RF and is not a good higher fidelity benchmark for evaluating the accuracy of CoCiP's parameterization-heavy approach.

Another issue with contrail models is that there have been limited efforts to validate their results or calibrate their parameterizations with observational data. Currently, analysis comparing contrail model outputs to observations of contrails [10] suggest that CoCiP produces contrails with properties within the range of in-situ measurements and remote sensing observations. However, these outputs do not compare CoCiP outputs to contrail observations on an individual basis, and the high degree of variability in observations means that this comparison provides only a weak assessment. This is a problem because if contrail models are to be used in contrail impact mitigation strategies for a flight, they should be able to predict the contrail impacts of that specific flight to some level of accuracy. In particular, the models must be shown to accurately reproduce trends due to differences in ambient parameters. APCEMM and other contrail models have similarly been the subject of few comparison studies.

Moreover, there are uncertainties in contrail modeling due to both the limitations of the contrail models themselves and the weather data inputs used in the models. The output of a contrail model can be very sensitive to the ambient conditions. The grid spacing and timesteps used in weather data sources, such as forecast and reanalysis models, are large relative to the size and lifetime of a typical contrail. This results in a mismatch between the fidelity of data requested by the contrail model and that which is provided by the weather data source. There been very few attempts to quantify the effects that systematic biases present in commonly used weather data products such as the ERA5 reanalysis model [11] have on the outputs and accuracy of contrail models. This could be due the number of confounding factors between the weather data error, modeling errors, and lack

of observations and measurements paired to specific flights.

A possible method to resolve this is to infer the likely weather parameters for an observed contrail, using a contrail model. When performed over a set of many contrails, this results in distributions of the ambient conditions as "inferred" by the models. A comparison of these inferred distributions to those observed by radiosonde measurements in literature can provide insight into the biases present in the weather data and contrail models. If the inferred distributions with either model agree with the radiosonde measurements, this provides evidence that the model physics are consistent with observations. Furthermore, any remaining error must reflect shortcomings in the model. Disagreement between the inferred meteorological data and the reanalysis data may also indicate systematic biases therein, and therefore avenues to address these biases. This would allow for studies where the errors attributable to weather data uncertainty are likely reduced, allowing for a better estimate of the errors due to modeling assumptions.

Having established these research gaps, this thesis aims to advance the contrail modeling field in three ways. First, APCEMM is improved to run faster with more efficient numerical algorithms and account for more physical processes that affect contrail behavior. This is for the purposes of having a viable higher order model reference on a large-scale study. Second, observations of contrails known to have been formed by specific flights are directly compared outputs from APCEMM and CoCiP. This comparison is to assess the models' abilities to replicate observations and to calibrate parameterizations for quantities such as the initial depth. Finally, an ambient parameter inference framework is developed to analyze 1) biases in the ERA5 weather data, 2) the differences in sensitivities to input parameters between APCEMM and CoCiP, and 3) the impacts the weather data error and modeling error each have on model estimates of contrail properties and climate impacts.

1.1 Basics of Contrail Physics

Contrails form due to the mixing of the warmer, moister engine exhaust and the cooler, drier ambient air. If the relative humidity of the plume becomes supersaturated with respect to water at any point during the mixing process, it is believed that the excess water vapor will condense onto soot

particles emitted from the engine exhaust. These newly formed droplets will then freeze, forming ice crystals. This condition for contrail formation is the Schmidt-Appleman criterion (SAC) [12]. For contrails to persist in the atmosphere after satisfying the SAC and initially forming, the ambient relative humidity with respect to ice (RH_i) must be supersaturated (greater than 100%), or else the newly formed contrail will sublimate within minutes.

The lifetime of a contrail can be split into three phases: the jet phase, the vortex phase, and the dispersion phase. During the jet phase, the pair of counter-rotating wingtip vortices interacts with the exhaust plume and causes the entrainment of humid ambient air, resulting in ice crystal growth. This process occurs on the timescale of about 10 seconds [13]. Next, the vortices descend in altitude due to the downwards velocity they exert on each other. During this descent, a fraction of the ice crystals will sublimate due to adiabatic heating [14].

Afterwards, the vortex structures collapse due to complex instability processes at a timescale of about 100 seconds [13], and the contrail enters the dispersion phase. In this phase, the contrail acts as a air mass that can expand to widths of multiple kilometers through diffusion and wind shear. It will mix in ambient air, which causes ice particle growth if the ambient air is supersaturated with respect to ice. It may also grow in depth due to gravitational settling of larger ice crystals out of the contrail core, forming a "fallstreak". The persistent contrail reaches its end of life when the ice crystals have fallen out of the ice supersaturated layer (ISSL) of the atmosphere due to gravitational settling or have sublimated due to the contrail air mass mixing in dry ambient air.

1.2   Factors Impacting Contrail Evolution

The evolution of a contrail is influenced by a number of atmospheric conditions and aircraft parameters. The atmospheric conditions include the RH_i, the wind shear, the ISSL depth, and the temperature. Large eddy simulations (LES) have shown that a higher RH_i results in a faster rate of ice crystal growth [7] [9] and a higher number of ice crystals surviving the vortex phase [15], both of which are correlated to the RF impacts. A larger ISSL allows the crystals to fall for a greater

distance without sublimating, increasing optical depth and allowing wind shear to spread the contrail over a farther distance. Wind shear is what primarily drives contrail expansion and increases the rate of ice crystal growth due to spreading the contrail thin and reducing competition for water vapor between individual ice crystals. However, its effect on contrail RF is less clear due to this increased ice growth also making particles settle out of the contrails faster, reducing contrail lifetime [9]. The temperature is a factor in determining the ice particle survival fraction during the vortex phase and therefore the overall lifetime of the contrail [15].

There are other factors that may impact the evolution of a contrail. This includes the vertical wind speed, which may counteract or hasten the settling of contrail ice particles into an ice subsaturated region [7]. Moreover, vertical advection causes changes in the density of air, which changes the shape of the contrail. Atmospheric turbulence and gravity waves also affect contrail lifetime behavior, partially from inducing a temperature fluctuation. This fluctuation causes perturbations in the RH_i field, which Lewellen (2014) found to promote the growth of larger ice particles over smaller particles and decrease contrail lifetime [9]. Aircraft geometry and emissions parameters also affect the evolution of a contrail. These include the soot, or non-volatile particulate matter emissions index (EI_{nvPM}), air speed, aircraft mass, wingspan, fuel flow rate, and potentially the fuel sulfur content [16].

1.3   Existing Contrail Models

Prior to APCEMM [3], contrail models could be categorized into the lower fidelity models, such as CoCiP [2], and expensive LES models [7][9], which resolve the transport phenomena to very fine spatial and temporal scales. LES models are typically used for parametric studies where sensitivities to specific input parameters are varied, rather than with real flight track and weather data. This is due to LES models being very computationally expensive, with a single simulation of a contrail taking many hours or days to finish, making them less suitable for large-scale studies.

APCEMM was developed to serve as a middle ground on the fidelity spectrum between CoCiP and LES models, providing a higher-order option compared to CoCiP for large-scale studies. It uses

a 2-D grid, explicitly simulating the transport and mixing of the contrail while featuring a binned ice microphysics scheme. However it has limitations making it unsuitable for that role, such as it slow runtime, non-physical boundary conditions, and ignoring of parameters such as atmospheric turbulence, updrafts, and the initial contrail aspect ratio.

1.4 Weather Data and Uncertainties in Contrail Modeling

A critical source of uncertainty in contrail modeling is the weather data. The most widely used dataset is the ERA5 reanalysis pressure levels data [11], which has a vertical resolution of approximately 1 km at cruise altitudes, a spatial resolution of approximately 30 km, and a temporal resolution of 1 hour. The data contains information about the vertical RH_i profile, the wind speeds, and the temperature, which can be used as inputs for contrail models.

This coarse spatiotemporal resolution relative to typical sizes and lifetimes of contrails along with limitations in the weather models themselves result in uncertainties in the ambient parameters. In particular, the vertical profile of RH_i is uncertain due to the coarseness of the ERA5 grid spacing relative to the size of ice supersaturated regions, which typically have widths on the order of 100 km [17] and depths on the order of 500 m [18]. Furthermore, profiles of RH_i may have large gradients, making subgrid models for RH_i difficult to develop and evaluate. Studies also suggest that the ERA5 model itself may have inherent biases such as over-predicting the formation of persistent contrails [19] and underpredicting the magnitude of wind shear [20].

1.5 Current Contrail Observation and Model Validation Efforts

Existing observations of contrails include in-situ measurements of bulk contrail properties [21][22] and remote sensing observations. In-situ measurement data play an important role in informing parameterizations of early-stage (age < 1000 s) contrail ice physics and providing points of comparison for quantities such as ice crystal number and particle radius distributions. However, they do not provide information on the geometry of the contrail and are primarily performed on contrails under

14

1000 seconds in age. The are some in-situ observations of aged contrails such as those observed in the ML-CIRRUS campaign [23], but those suffer from a small sample size and a lack of information regarding the geometry of the contrail. Remote sensing observations such as those performed by Minnis et al. (2002) [24] during the 2001 air traffic shutdown have been able to estimate the width, depth, and optical depth of aged contrails up to 40 km in width. However, these observations are not attributed to individual flights, making their initial conditions difficult to evaluate.

Efforts to compare contrail model outputs to observations have been limited. Schumann et al. (2017) shows that the CoCiP model produces a range of outputs in key bulk contrail properties as a function of contrail age that covers the range of in situ and remote sensing observations, but does not compare model outputs to observations on an individual contrail basis. The range of key contrail properties such as optical depth, ice particle number, width, and depth for a contrail of a given age can vary by orders of magnitude, so these comparisons do not provide narrow bounds on contrail model performance and the uncertainties associated with the models. Naiman et al. (2011) [25] compares the results of their LES simulation to these in-situ and remote sensing observations, but the comparisons are likewise not on an individual contrail basis.

1.6   Objectives of the Thesis

Considering these research gaps in contrail modeling, this thesis aims to achieve three primary objectives:

1. Improve the algorithmic efficiency and representation of contrail physics within APCEMM. More specifically, APCEMM should be able to:

    (i) Complete a 3-hour simulation of a contrail within 5 CPU minutes and a 10-hour simulation within 60 CPU minutes.

    (ii) Capture the effects of turbulence-induced temperature fluctuations and vertical advection on contrail ice physics and lifetime.

    (iii) Improve APCEMM's parameterization for the initial contrail depth through calibration on a set of 152 flight-attributed LIDAR observations.

15

2. Evaluate the abilities of APCEMM and CoCiP to reproduce contrails in properties such as depth, width, and optical depth on an individual contrail basis by comparing to the same LIDAR observations.

3. Use distributions of ambient ISSL depth, wind shear, and RH_i as inferred by contrail models to study the sensitivities of models to input parameters, analyze biases in the ERA5 weather data, and quantify differences in overall contrail RF due to weather data uncertainty and modeling assumptions.

2 Methods

2.1 Updates to APCEMM

2.1.1 Initialization of the Contrail Plume

Preliminary comparisons of APCEMM's estimates for contrail width and depth to the LIDAR observations confirmed that it underestimated the initial contrail depth and overestimated the initial contrail width. CoCiP's parameterizations of the initial width and depth are used to estimate the aspect ratio, and the final plume area from the early plume model within APCEMM is used to then calculate the initial width and depth. I also implement new shifting and scaling factors to operate on the initial aspect ratio as estimated by the CoCiP method, enabling calibration using LIDAR observations.

The depth and width used to initialize the aspect ratio, D_A and W_A, are defined as a shifting-scaling operation on the depth and width the CoCiP model uses, D_C and W_C:

$$D_A = A_D + B_D \times D_C \tag{1}$$

$$W_A = A_W + B_W \times W_C \tag{2}$$

where A_D, B_D and A_W, B_W are the shifting-scaling parameters for the width and depth respectively.

Since the initial contrail plume is assumed to be an ellipse, the initial characteristic depth and width D_0 and W_0 are then:

$$D_0 = 2 \times \text{AR} \times \left(\frac{A_P}{\pi \times \text{AR}} \right)^{\frac{1}{2}} \tag{3}$$

$$W_0 = \frac{D_A}{\text{AR}} \tag{4}$$

where AR is the aspect ratio defined as D_A/W_A and A_P is the end of vortex phase plume area as calculated by the APCEMM's early plume model.

The ice particles from the end of the early plume model are then initialized on the grid at an altitude calculated from APCEMM's vortex sinking parameterization. The particles are spatially distributed assuming a 2-D Gaussian distribution with standard deviations in the particles' x and y coordinates σ_x, σ_y are defined as:

$$\sigma_x = \frac{W_0}{8} \tag{5}$$

$$\sigma_y = \frac{D_0}{8} \tag{6}$$

I also experiment with the shape and ice crystal distribution of the initial plume. LES results [7], [9] suggest that contrail plumes in the early stage ($t \leq 2000$s) have complex shapes often inadequately represented by an ellipse. Simulations of the vortex phase show a primary and secondary wake where ice crystals are bimodally distributed in altitude [26]. However, changing the initial shape or vertical particle distribution did not cause significant differences in the behavior of contrails, with diagnostics such as the time-integrated ice mass differing by less than 5% for a 12-hour simulation. I therefore retain the assumptions of an initially elliptical plume with a 2-D Gaussian spatial particle distribution. The results of calibrating (A_D, B_D) with LIDAR observations are described in Section 3.1

2.1.2 Temperature Perturbations

APCEMM is updated to simulate some effects of atmospheric turbulence and gravity waves through the inclusion of periodic fluctuations in the ambient temperature. The 2-D temperature field $T(x, y)$ is perturbed, using the expressions proposed by Lewellen (2014) [9]:

$$T'(x, y) = T(x, y) + \epsilon_1(x, y)\epsilon_2(x, y)T_{\mathrm{amp}} \tag{7}$$

where $T'(x, y)$ is the perturbed temperature field, $\epsilon_1(x, y)$ and $\epsilon_2(x, y)$ are uniform random variables between -1 and 1 independently generated at each grid point, and T_{amp} is the amplitude of the temperature perturbation. This perturbation is changed every t_{add} seconds in the simulation. The magnitude of the atmospheric turbulence and gravity waves simulated depends on the selection of T_{amp} and t_{add}, where higher T_{amp} and lower t_{add} indicate greater intensity.

The ice particle number and ice mass decrease as a function of time when the turbulent temperature fluctuations are increased, as seen in Figure 1. Lewellen (2014) found that increasing the turbulent temperature fluctuation amplitude from 0.2 K to 2 K can cause a decrease of the ice particle number at $t = 2 \times 10^4$ seconds by approximately an order of magnitude (i.e. 90%). APCEMM finds a comparable decrease of 87% in the ice particle number at $t = 2 \times 10^4$ seconds, with an associated 54% reduction in the full-lifetime integrated optical depth.
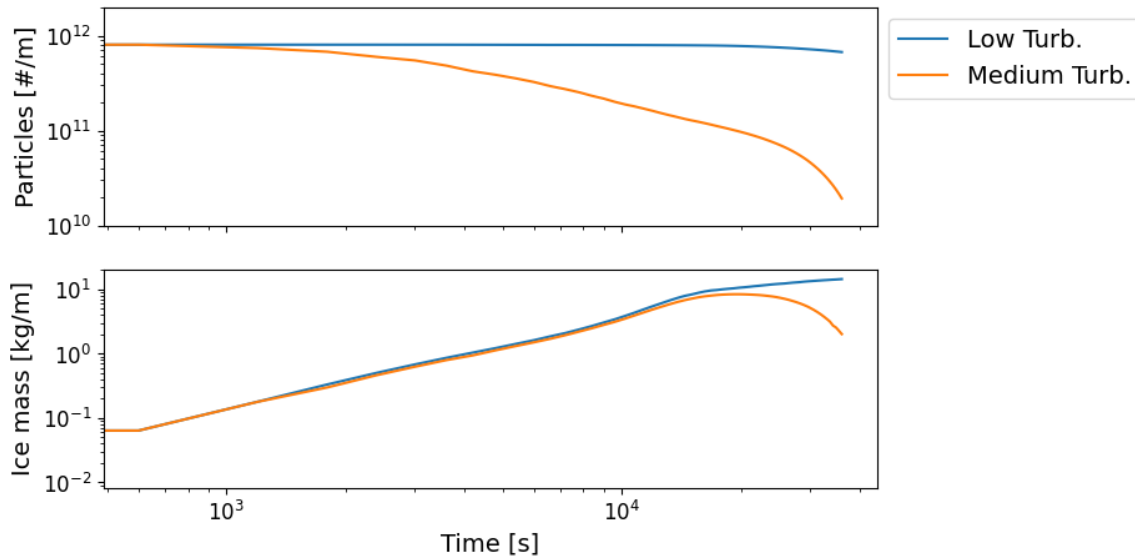
Figure 1: Effect of turbulent temperature fluctuations on ice particle number and ice mass on a contrail. "Low Turb." uses $T_{amp} = 0.2$ K, while "Medium Turb." uses $T_{amp} = 2.0$ K. Both cases use $t_{add} = 10$ min. The simulations are performed assuming $RH_i = 110\%$, shear $= 0.002$ s^{-1}, T = 217 K, and $EI_{nvPM} = 10^{14}$ particles / kg fuel.

For all subsequent simulations in this thesis, the temperature perturbations are turned off due to difficulties in inferring a level of atmospheric turbulence in the ERA5 data. This adds an additional confounding source of uncertainty that requires an in-depth analysis and would be a interesting topic for a follow-up study. This assumption of zero temperature fluctuations leads to APCEMM estimating higher values in optical depth, contrail lifetime, and RF. However, this does not affect our conclusions when comparing APCEMM and CoCiP, since the CoCiP-estimated particle losses from temperature fluctuations induced by mesoscale turbulence and gravity waves are very small, as seen in Figure 16 in Schumann (2012) [2].

2.1.3 Changes to the Transport Solver

The spectral solver in APCEMM, while efficient, relies on non-physical periodic boundary conditions and a fixed grid size which must be large enough to accommodate the maximum extent of the contrail. I therefore replace it with a finite-volume scheme that uses a semi-implicit Strang operator splitting approach [27]. The advection is solved to the half-timestep with an explicit scheme, followed by

implicit diffusion for the full timestep, finishing with explicit advection for the last half-timestep. The min-mod flux limiter [28] is used to calculate the ice particle and mass fluxes at the cell faces and minimize truncation error while preserving monoticity in the ice number and volume fields. This change in solver addresses the issues above. Additionally, this removes the expensive calculation of the discrete Fourier transform associated with every new grid size and domain, allowing for the introduction of algorithms that optimize APCEMM's runtime through adaptive grid spacing and sizing, as described below.

2.1.4 The LAGRID Algorithm

Having replaced the spectral solver, APCEMM is now free to adapt the grid spacing and domain size every time step to the extent of the contrail and improve runtime. To achieve this, I implement the LAGRID algorithm.

The first step is to split the grid into cells that were considered inside the contrail and cells that were not. This tracks the contrail as an expanding control volume as processes such as diffusion, wind shear, ice growth, and vertical advection act on the contrail. A cell is considered "inside" the contrail boundaries if the ice particle number density in that cell is greater than 10^{-5} times the maximum ice particle number density in the domain.

After simulating the transport, ice growth, and vertical advection for a given timestep, the grid spacing Δx, Δy for the following timestep is computed. This spacing adapts to the size of the horizontal and vertical extents of the contrail to ensure at least 50 cells in both directions within the contrail and increases with the contrail size up to a maximum of $\Delta x = 50$ m and $\Delta y = 7$ m. The cells considered "inside" the contrail are first remapped onto a rectangular grid with the same width and depth dimensions as the contrail. Finally, buffers are added to the new grid to allow the contrail to shear, diffuse and settle. The sizes of these buffers B_{top}, B_{bot}, B_{left}, and B_{right} (in meters) are calculated as follows:

$$B_{\textbf{top}} = \max(100, \sqrt{\mathcal{D}_Y \Delta t}) \tag{8}$$

20

$$B_{\textbf{bot}} = \min(300, \sqrt{\mathcal{D}_Y \Delta t} + v_{\text{fall}} \Delta t) \tag{9}$$

$$B_{\textbf{left}} = \frac{sD\Delta t}{2} + \sqrt{\mathcal{D}_X \Delta t} \tag{10}$$

$$B_{\textbf{right}} = \frac{sD\Delta t}{2} + \sqrt{\mathcal{D}_X \Delta t} \tag{11}$$

where $\mathcal{D}_X, \mathcal{D}_Y$ are the diffusion coefficients, Δt is the time step, s is the wind shear, D is the total contrail depth, and v_{fall} is the settling velocity of the largest particles in the contrail.

As seen in Figure 2 below, the LAGRID algorithm results in runtimes over 20 times faster for a 3-hour simulation, with a runtime of 25.52 seconds compared to the 528.7 seconds required when performing APCEMM simulations with a fixed grid size. The benefit of LAGRID decreases with contrail age due the the contrail expanding in size, but due to earlier time savings and a coupling between the grid domain and the contrail size, LAGRID is still 3.8 times faster than the fixed grid method for a 10-hour simulation, with a runtime of 555.4 seconds versus 2128 seconds.
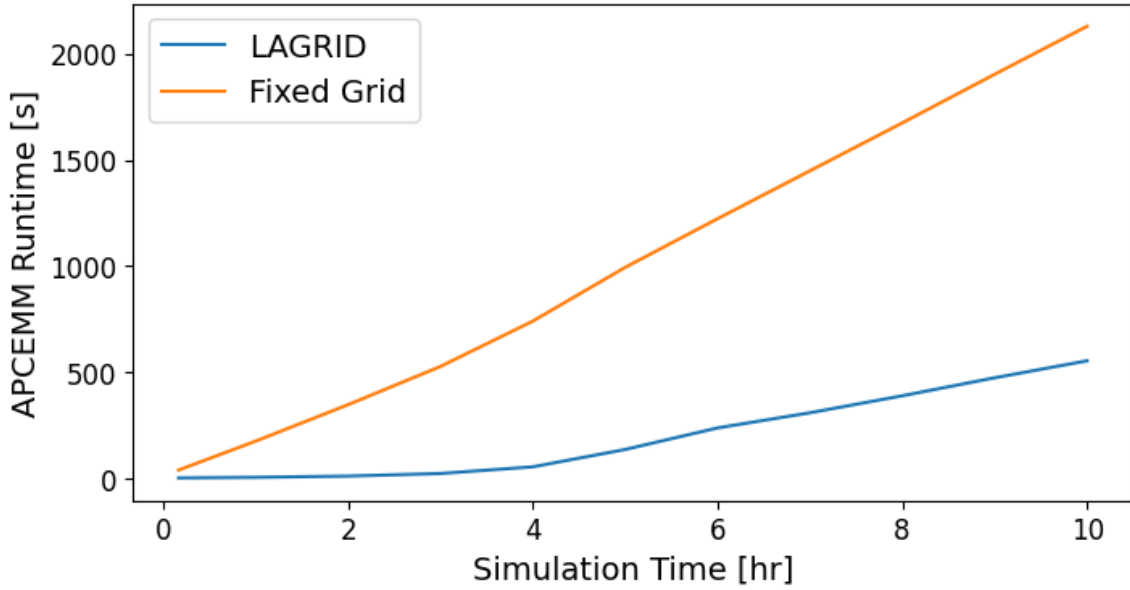
Figure 2: APCEMM runtimes with LAGRID and fixed grid methods using 8 CPU cores

2.1.5 Vertical Advection

When the contrail is advected upwards or downwards due to the vertical wind speed, the air density changes. This causes the contrail to expand or contract and alter its shape. These changes in the contrail shape are accounted for by tracking the vertical and horizontal extent of each row within the domain and remapping the grid cells to a new grid at the end of the process, as depicted in Figure 3. This remapping introduces some artificial diffusion at each time step because of the imposition of structured grid boundaries on the new contrail shape. However, this effect can be reduced by lowering the maximum grid spacing $(\Delta x, \Delta y)$, and a grid independence study showed that a 12-hour simulation using $(\Delta x, \Delta y) = (50 \text{ m}, 7 \text{ m})$ showed a less than 2% difference in time-integrated contrail ice mass compared to the same simulation using $(\Delta x, \Delta y) = (25 \text{ m}, 3 \text{ m})$, suggesting that our choice in $(\Delta x, \Delta y)$ results in minimal artificial diffusion effects.
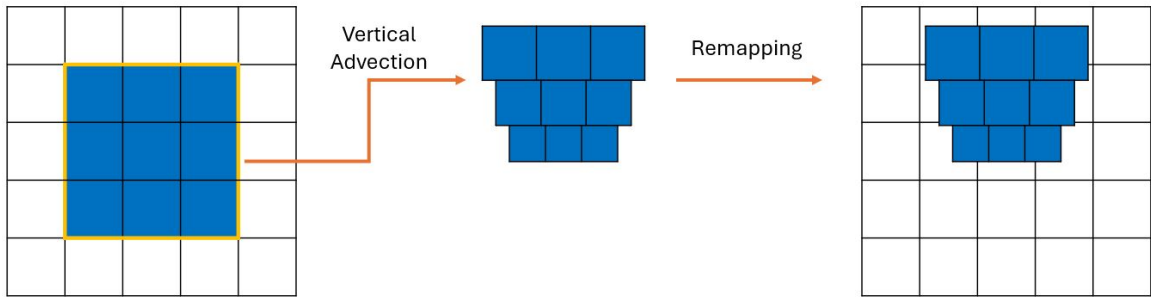
Figure 3: Illustration of the grid cell size adjustment and remapping processes for vertical advection

2.2 Calibration of Contrail Models with LIDAR Observations

2.2.1 Obtaining Flight Attributed LIDAR Extinction Cross Sections

The process for obtaining the set of flight attributed CALIOP L2 LIDAR [29] observations of contrail cross sections involves four steps in the following order: contrail detection, flight attribution, cross section extraction, and extinction retrieval. This process is illustrated below in Figure 4.
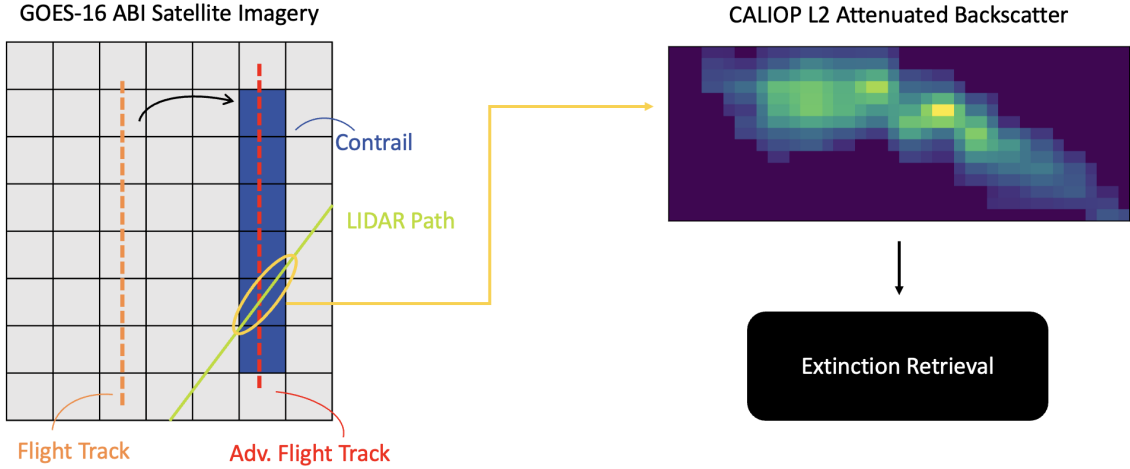
Figure 4: Process for obtaining flight attributed contrail cross sections

First, a large number of contrails are detected on the GOES-16 ABI [30] geostationary satellite imagery using a a convolutional neural network described in Meijer et al. (2022) [31]. To eliminate false positives, these detections are then manually verified before being passed on as candidates for flight attribution. To perform flight attributions, flight tracks are first advected using the ERA5 reanalysis wind data. In the case of an intersection of the advected flight track with a detected contrail in geographic coordinates, the CALIOP L2 LIDAR data is scanned for an intersection with the contrail. If a detected contrail both has an attributed flight and is covered by the LIDAR data, a height estimation algorithm described in Meijer (2024) [32] is applied on the geostationary satellite image of the contrail to verify that the contrail is at the same altitude as observed by the LIDAR. This is to avoid incorrect attributions in the case that there are multiple contrails spatially close to one another. If the estimated height shows agreement with the altitude provided by the LIDAR, the flight attribution process is complete, and I extract the attenuated backscatter cross section of the contrail from the LIDAR data.

However, the quantity of interest is the extinction χ of the contrail cross section, as it is needed to compute the optical depth. The extinction is directly proportional to the attenuated backscatter β via the LIDAR ratio S:

$$\chi = S\beta \tag{12}$$

This LIDAR ratio S can be extracted from the CALIOP L2 profiles using the HERA algorithm as described in Young and Vaughan (2009) [33]. With the 2-D extinction cross section of the contrail, a direct comparison between the LIDAR cross section and the APCEMM and CoCiP results can be performed.

2.2.2 Metrics for Comparing Cross Sections

In order to compare two different extinction cross sections, there needs to be metrics on which the two cross sections are compared. I choose three contrail properties as metrics: the width W, the depth D, and the integrated optical depth (IOD) τ_{int}. Comparing the width and depth of the contrail facilitates the evaluation of contrail models' abilities to reproduce contrails of similar spatial scales to observations, while the IOD serves as a metric correlated with the ice mass and RF (i.e. climate impact) of the contrail independent of the time of day and season.

I define the depth D as the difference between the maximum and minimum altitudes in which there exists a point in the contrail where the extinction is greater than the 10^{-1} times the maximum extinction in the contrail. The width W is defined analogously to the depth. For a 2-D extinction field $\chi(x, y)$, the IOD τ_{int} is defined as

$$\tau_{\text{int}} = \int_{x_{\min}}^{x_{\max}} \tau_y \ dx \tag{13}$$

where τ_y, the vertical optical depth, is defined as:

$$\tau_y = \int_{y_{\min}}^{y_{\max}} \chi(x, y) \ dy \tag{14}$$

The CoCiP model does not output a 2-D extinction field, but outputs a representative dimensionless contrail optical depth τ_{contrail} and width W. For the CoCiP output, the IOD is calculated

as the product of the width and the representative optical depth:

$$\tau_{\text{int}} = W \times \tau_{\text{contrail}}$$

The values of D, W, τ_{int} obtained from APCEMM and CoCiP simulations are compared to the LIDAR measurements in a percent error sense. These percent differences will be called $\epsilon_D, \epsilon_W, \epsilon_\tau$, defined as follows:

$$\epsilon_X = 100 \left| \frac{X_M - X_L}{X_L} \right| \tag{15}$$

where X is any given parameter of the contrail and the subscripts M and L refer to that for the contrail model (i.e. APCEMM or CoCiP) output and the LIDAR observation respectively.

2.2.3 Using ERA5 Weather Data Input with APCEMM

For each flight attributed to a specific contrail captured on the CALIOP L2 LIDAR, the results output by APCEMM are compared against the observations. The flight data (longitude, latitude, altitude, time, heading, ground speed) are obtained through the OpenSky database. The ambient meteorological conditions, including the temperature, wind shear, and humidity, as a function of time are estimated by advecting the flight waypoint through the ERA5 reanalysis wind data. The soot particle emissions index EI_{nvPM} is assumed to be 10^{15} particles per kg fuel.

The temperature field is linearly interpolated in both time and altitude. A single value for the wind shear, linearly interpolated in time and altitude, is used. The humidity profile is linearly interpolated in time, but nearest neighbor interpolation is used for determining the vertical profile. This is due to the prevalence of large gradients in the vertical humidity profile, as observed in radiosonde measurements [34]. Therefore, using linear interpolation could lead to systematic underestimations of the ISSL depth. For the first timestep, the humidity is scaled using Equation 1 in Teoh et al. (2022) [4] to account for biases in ERA5 against ice supersaturated regions when it is known a contrail formed. However, the humidity for subsequent timesteps, when the contrail has grown to a more similar length scale compared to the grid spacing of ERA5, is taken directly from the ERA5

data.

2.2.4 Calibration of Initial Depth Estimation Parameters

The LIDAR cross sections are first employed to calibrate the initial depth estimation parameters A, B as described in Equation 1. The contrail depth is the first metric targeted for calibration due to its effects on the evolution of the contrail's width and optical depth. Furthermore, the uncertainty in the observed contrail depth from the LIDAR cross sections is limited to the vertical resolution of the LIDAR, which is approximately 50 meters. In contrast, uncertainties in the LIDAR intersection angle and the LIDAR ratio arising from the flight track advection and extinction retrieval processes are not as concretely quantifiable. Therefore, the uncertainties in the widths and optical depths of the LIDAR cross sections are likely greater than those for the depths.

The weather data input affects the results of the depth calibration due to the variability of the ISSL depth. As such, the calibration results using two methods of weather data input are compared. First, the simulations over all flights are performed using the ERA5 reanalysis data as-is, and A, B are tuned to minimize the percent depth error over the sample of contrails that form. Second, a case with constant ambient parameters is considered. RH_i is set to a 110%, the temperature is set to 217K, the wind shear is set to 0.002 s^{-1}, and the ISSL depth is set to 280 m, one half the mean ISS layer depth as measured by radiosondes in Spichtinger et al. (2003) [18]. The optimization process is then repeated using this input.

If there is a disagreement between the calibration results, it may suggest that there are systematic biases in the ERA5 humidity profiles for cases where $RH_i > 100\%$, or that variations in the humidity profile have asymmetric effects on the resulting contrail depth. EI_{nvPM} is assumed to be 10^{14} particles per kg fuel for both approaches. This is a different than the typical value of 10^{15} in subsequent experiments in this thesis, but since the gravitational settling timescale is long compared to the ages of the contrails observed (typically under 1 hour), we do not expect this difference to have a major effect on the calibration results.

The objective of the calibration is to find a combination of (A, B) that reduces $\overline{\epsilon_D}$, the percent error in contrail depth from observation averaged over all cases. For both calibration methods, a grid search is performed, where A is varied over the domain $[0, 300]$ with increments of 25 meters, while B is varied over $[0, 2]$ with increments of 0.25. The results are shown in Section 3.1.

2.3 Inferring Ambient Meteorological Parameters with Contrail Models

2.3.1 Optimization Problem

For each flight, the task of inferring the ambient conditions necessary to reproduce a contrail observation with a model is framed as an optimization problem where the objective is the minimize the loss function L, equal to the sum of the absolute percent differences in width, depth, and IOD. This forces the optimizer to weigh the percent errors in all three metrics equally and select the combination of parameters that produces a contrail geometrically and optically similar to the observation.

$$L(D_{\text{ISS}}, s, \text{RH}_{\text{i}}) = \epsilon_D + \epsilon_W + \epsilon_\tau \tag{16}$$

Each iteration in the optimization process consists of three steps. Suppose that $\vec{x} = (D, s, q)$, is the guess for the optimal parameters, where D, s, and q are the guesses for the ISSL depth, wind shear, and RH_{i} respectively, and that $\vec{x_0} = (D_0, s_0, q_0)$ is the guess at the start of the iteration. First, I perform a grid search for the ISSL depth D_{min} that minimizes ϵ_D while assuming $s = s_0$ and $q = q_0$. If multiple values of D yield the same local minimum ϵ_D, the smallest value is chosen as D_{min}. I then perform a grid search for s_{min}, the wind shear value that minimizes ϵ_W while using $D = D_{\text{min}}$ and $q = q_0$. I perform a final grid search for q_{min}, the value of RH_{i} that minimizes ϵ_τ given $D = D_{\text{min}}$ and $s = s_{\text{min}}$. The values $(D_{\text{min}}, s_{\text{min}}, q_{\text{min}})$ are then used as the initial guess for the next iteration. This process is repeated until the loss function is below 1%, or the maximum number of allowed iterations (7) is reached. The constraints on D_{ISS}, s, and RH_{i} are [10 m, 2000 m], [0 s^{-1}, 0.03 s^{-1}], and [100%, 160%] respectively. Figure 5 is a simplified schematic describing this processes, with results shown in Section 3.2.
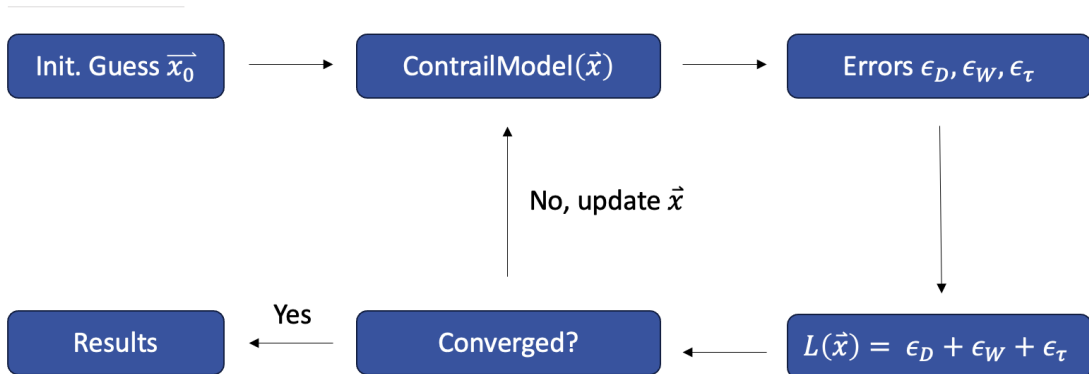
Figure 5: Flowchart for ambient parameter optimization

2.3.2 Analysis using Ambient Parameter Distributions

The distributions of inferred ambient parameters are then used to examine the sensitivities of APCEMM to input parameters such as the ambient temperature T, depth estimation parameters (A, B), and the soot particle number emissions $\mathrm{EI_{nvPM}}$. The distributions illustrate the interactions between the aforementioned input parameters and the inferred ambient ISSL depth, wind shear, and $\mathrm{RH_i}$. The cases considered for this study are listed below in Table 1.

Table 1: APCEMM Cases considered for case-by-case ambient parameter optimization problem

Case Name	A [m]	B [-]	T [K]	$\mathrm{EI_{nvPM}}$ [#/kg]
Base	50	1	217	10^{15}
HiTemp	50	1	222	10^{15}
LowSoot	50	1	217	10^{14}
HiDepth	200	0.75	217	10^{15}

The inferred distributions are then used to analyze biases and errors in the weather data and contrail models. Distributions from ambient parameter inference using APCEMM and CoCiP are compared to each other, radiosonde measurements, and the ERA5 weather data. The means, medians, and standard deviations of the distributions will serve as the metrics for comparison. These distributions, with the radiosonde data as the ground truth, can be used to analyze model sensitivities (Section 3.2), biases in the ERA5 data (Section 3.3), and the relative magnitudes of errors from

weather data uncertainty and modeling assumptions (Section 3.4).

2.4 Quantifying ERA5 Data and Modeling-Related Errors

In order to quantify errors arising from uncertainty in the ERA5 data versus errors that arise from modeling assumptions made in lower-order models such as CoCiP, there needs to be a case where the errors from the ERA5 data are minimized, as well as a case where errors in the weather data are minimized. The errors when using the higher order APCEMM model with the ERA5 data serve as a measurement of the error attributable to the weather data when using a higher order model, while the errors from CoCiP when using the APCEMM-inferred ambient parameters is a measurement of the error due to the modeling assumptions made in CoCiP. Table 2 below lists the simulations performed for this analysis.

Table 2: APCEMM and CoCiP cases for quantification of modeling and weather data error. Descriptions of APCEMM models are the same as in Table 1.

Case Name	Model	Weather Data
APC-Opt	APCEMM-HiDepth	APCEMM-HiDepth inferred
APCHD-E5	APCEMM-HiDepth	ERA5
APCB-E5	APCEMM-Base	ERA5
CoCiP-E5	CoCiP	ERA5
CoCiP-APCOpt	CoCiP	APCEMM-HiDepth inferred

For the CoCiP simulations, EI_{nvPM} is set 10^{15} particles per kg fuel, and the temperature set to 217 K when not using the ERA5 data. The ambient parameters as inferred by APCEMM are taken from those inferred by the HiDepth case as described in Table 1. The results are shown in Section 3.4.

2.5 Analysis of Lifetime and Radiative Forcing Implications

Finally, the lifetime RF impacts of the contrails are evaluated with APCEMM and CoCiP using both the ERA5 and the model-inferred ambient parameters. Table 3 describes the cases considered

for this analysis.

Table 3: Description of cases considered for RF analysis

Case Name	Model	Weather Data
APCB-ERA5	APCEMM-Base	ERA5
APCHD-ERA5	APCEMM-HiDepth	ERA5
CoCiP-ERA5	CoCiP	ERA5
APCB-Opt	APCEMM-Base	APCEMM-Base inferred
APCHD-Opt	APCEMM-HiDepth	APCEMM-HiDepth inferred
CoCiP-Opt	CoCiP	CoCiP inferred
CoCiP-APCOpt	CoCiP	APCEMM-HiDepth inferred

When using either the ERA5 or the inferred parameters, the simulation is allowed to run until the contrails reach the end of life conditions. For the inferred parameters cases, the ambient conditions are assumed to be constant. The CoCiP simulations end when the dimensionless optical depth is less than 10^{-6}, while the APCEMM simulations end when the total number of ice particles is less than 10^{-5} times the initial post-vortex sinking particle number. The ERA5 cases use time-dependent meteorological data, while the ambient conditions do not vary as a function of time for the inferred parameters cases. For the inferred parameter cases, the ambient temperature is set to 217 K and EI_{nvPM} is set to 10^{15} particles per kg fuel.

The metric for comparing the RF results of the models is the energy forcing (EF) per contrail length, defined as the integral over time of the net RF times the contrail width W:

$$EF = \int_{t_0}^{t_f} \text{RF}_{\text{net}}(t)W(t) \, dt$$

To maintain consistency, the net RF for both models at each time step is calculated using the methods employed by CoCiP. The CoCiP shortwave and longwave radiative forcing functions require a number of inputs that APCEMM does not directly produce: the habit weights that describe the shapes of ice crystals, a scalar dimensionless optical depth, and a scalar volume-averaged particle

radius. The habit weights are assumed to be the same as in CoCiP. The particle radius r and dimensionless optical depth τ are calculated as follows:

$$r = \frac{3}{4\pi}\left(\frac{V}{N}\right)^{1/3} \tag{17}$$

$$\tau = \frac{\text{IOD}}{W} \tag{18}$$

where V is the total ice per meter of the cross section, N is the total particle number per meter, and W is the contrail width. Although the area-weighted radius may be possibly more representative of the RF of the contrail, the volume-weighted ice particle radius is used to stay consistent with CoCiP's calculations.

3 Results and Discussion

3.1 Initial Depth Calibration with APCEMM

Calibrating the initial depth estimation parameters (A, B), as described in Equation 1, using the constant ISSL depth and ambient parameters as described in Section 2.2.4, results in $A = 50$ m and $B = 1$ as the optimal parameters (hereinafter the "const-optimized parameters"). In contrast, using the ERA5 data to minimize the average percent error $\bar{\epsilon}_D$ in contrail depth yields $A = 200$ m and $B = 0.75$ (hereinafter the "ERA5-optimized parameters"). The results of these calibrations as compared to the default APCEMM settings of $(A, B) = (0 \text{ m}, 1)$ are shown in Figure 6.
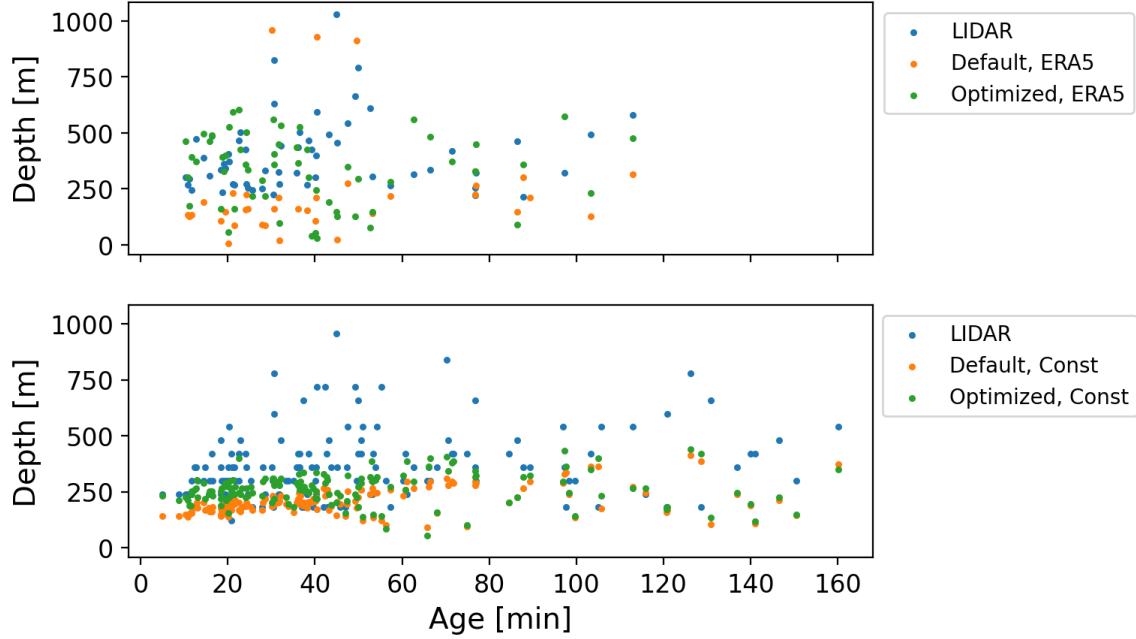
Figure 6: Scatter plot visualizing effects of initial depth calibration using the ERA5 data (top) and the constant ISSL depth = 280 m (bottom). For the ERA5 case, only LIDAR data points for which the optimized parameters formed a contrail that survived until the observed age are shown.

Both sets of optimized parameters result in an increase in predicted contrail depth and a decrease in $\bar{\epsilon}_D$. APCEMM using the default initial depth parameters $(A, B) = (0 \text{ m}, 1)$ consistently underestimates the contrail depth for both the ERA5 and constant cases, with a mean depth of 227 m with the ERA5 case and a mean of 260 m with the constant case compared to the mean LIDAR observed depth of 331 m. Using the ERA5 data with the default (A, B) results in an $\bar{\epsilon}_D$ of 56%, while using the ERA5 depth parameters results in an $\bar{\epsilon}_D$ of 48%. When using the constant ISS layer depth and ambient parameters, the default version of APCEMM yields an $\bar{\epsilon}_D$ of 41%, while using constant depth parameters results in an $\bar{\epsilon}_D$ of 37%.

However, these two different approaches with the weather data result in versions of APCEMM that produce contrails with different initial depths. When the ISSL depth is set to a high value of 1000 m to not be a limiting factor for contrail depth, APCEMM with the ERA5-optimized parameters produces contrails on average 64% deeper than APCEMM with the const-optimized parameters and

100% deeper than APCEMM with the default (A, B). Figure 7 illustrates the differences in contrail depth when using APCEMM with the different depth estimation parameters on a case with constant RH_i, shear, and a large ISSR depth of 1000 m.
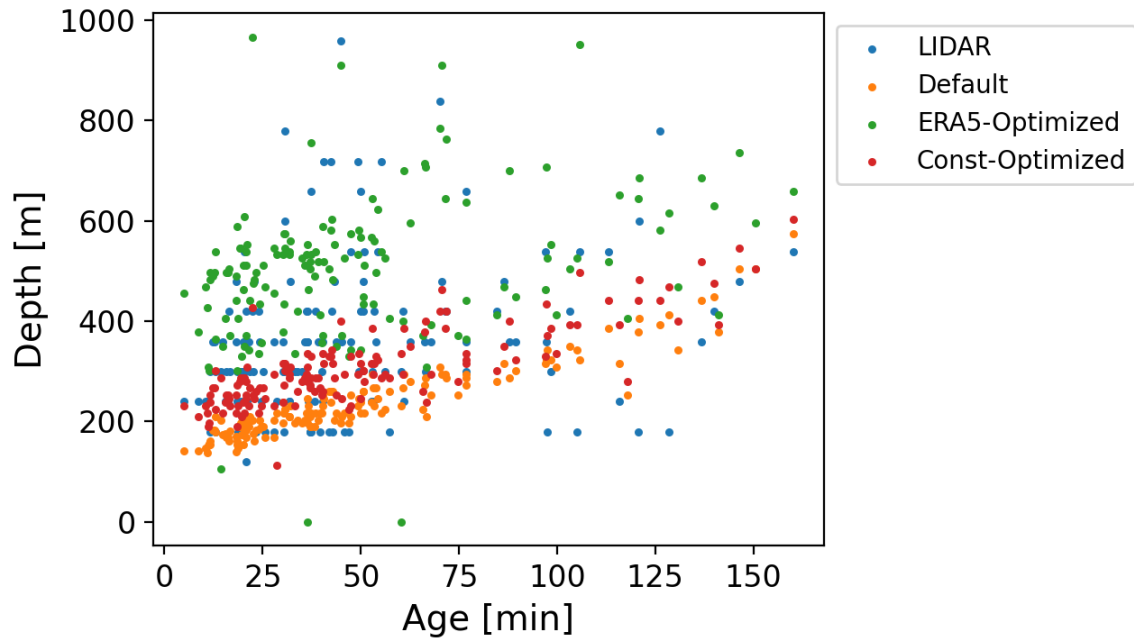
Figure 7: Scatter plot of results for the simulated contrail depth against the LIDAR cross section at the observed age using a constant $RH_i = 110\%$, ISSL depth of 1000 m, and wind shear = 0.002 s^{-1}. Blue: LIDAR; Orange: APCEMM w/ default parameters, Green: Parameters as optimized with ERA5 data; Red: Parameters as optimized with the constant ISSL depth case

APCEMM versions with lower values of A show a stronger correlation between contrail age and contrail depth. The default $(A, B) = (0 \text{ m}, 1)$ case results in an R^2 of 0.87 between age and depth, while the ERA5-optimized case yields an R^2 of 0.10 and the const-optimized case yields an R^2 of 0.67. This result is explained by the fact that the ERA5-optimized parameters predict a higher initial depth, so the percent difference between the initial contrail depth and the contrail depth at some later point in time is smaller.

33

The two methods of weather data input yield two versions of APCEMM that predict different initial contrail depths. Since there is no ground truth for the RH_i profile, it is difficult to say that one version has a better estimate of the initial depth than the other, although both outperform the original parameterization. Because the initial depth affects many contrail properties as a function of time, the subsequent studies will utilize these two versions of APCEMM and compare the impact of an increased initial depth on factors such as the inferred parameters using ambient parameter inference or the lifetime radiative forcing. APCEMM with the ERA5-optimized parameters and the const-optimized parameters are hereinafter referred to as "APCEMM-HiDepth" and "APCEMM-Base", respectively.

3.2 Ambient Parameters as Inferred by APCEMM and CoCiP

The distributions of the ISSL depth, wind shear, and RH_i as inferred by APCEMM and CoCiP using the ambient parameter inference framework described in Section 2.3 are illustrated in Figure 8.
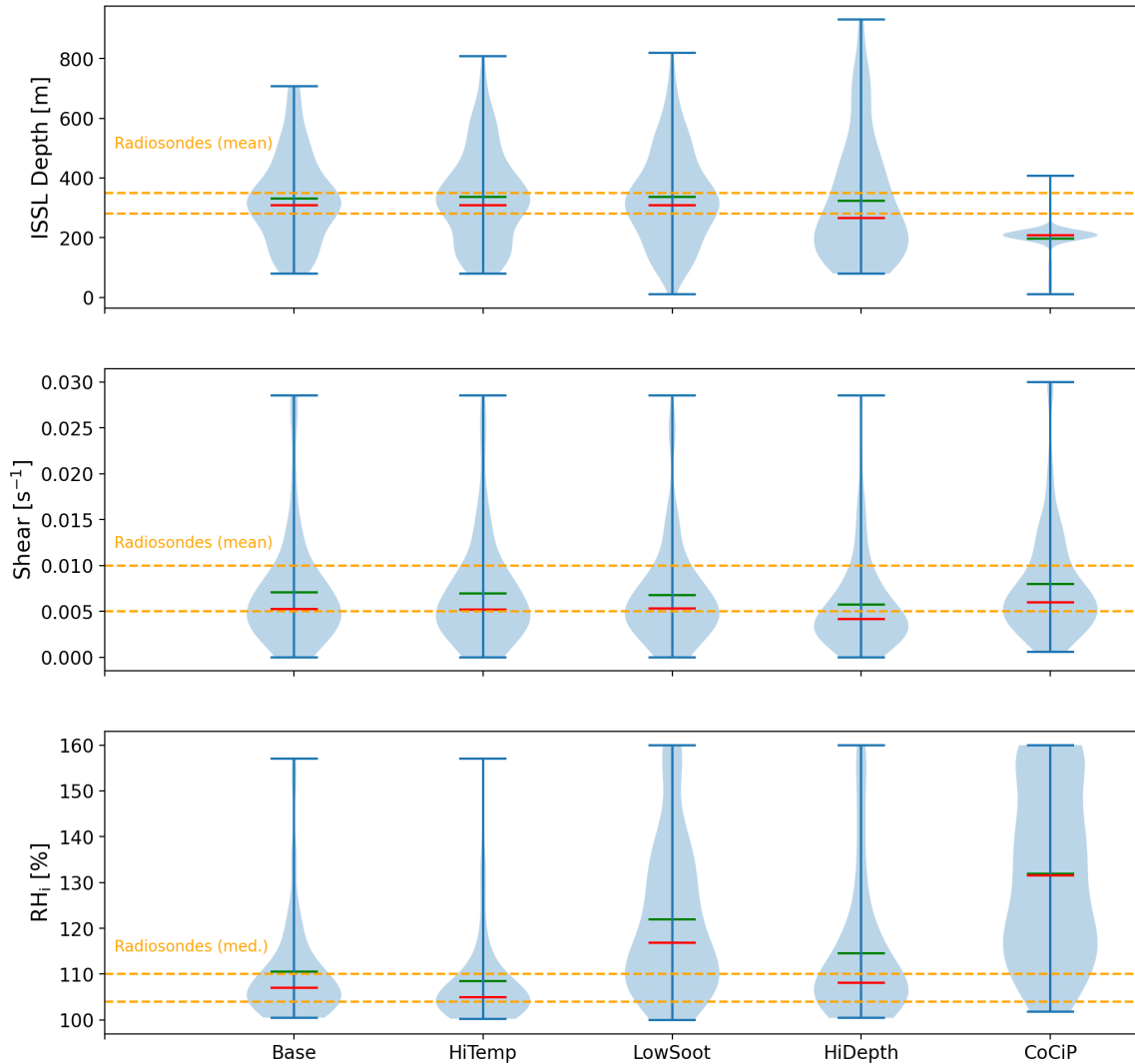
Figure 8: Distributions of the inferred ISSL depth (top), wind shear (middle), and RH_i (bottom) using CoCiP and APCEMM cases as described in Table 1. The green lines indicate the means of the distributions, while the red lines indicate the medians. Means and medians obtained from radiosonde measurements in literature are shown in orange.

3.2.1 APCEMM-inferred ISSL Depth

Changing the temperature or EI_{nvPM} does not significantly change the shape, median, or mean of the distribution of APCEMM-inferred ISSL depths. If the observed contrails were of an older age, EI_{nvPM} may play a larger role since simulations suggest that a lower EI_{nvPM} results in a faster

35

settling rate [9]. However, all contrails observed were less than 3 hours old, so there is insufficient time for contrail fallstreaks that settle for enough to cause EI_{nvPM} to make a difference.

However, the HiDepth case results in a distribution with more skewed towards lower depths, with a lower median of 266 m compared to the 309 m of the base case despite having a similar mean of 323 m vs the 332 m of the base case. This is due to APCEMM-HiDepth having fewer cases where it underestimates the initial contrail depth. With the base model, there are cases where APCEMM, irrespective of the ISSL depth, is unable to reproduce a contrail due to underestimation of the initial contrail depth. Nonetheless, the optimizer detects a small gradient relating ISSL depth and initial contrail depth, resulting in higher values in the inferred distribution.

The mean ISSL depths show some level of agreement with radiosonde measurements in literature, where the mean total ISSL vertical extents range from 560 [18] to 700 [35] m. If the extent of the ISSL below the flight level is assumed to be half the total vertical extent, both the base and HiDepth cases have their means within the the range of radiosonde measurements. The shape of the HiDepth distribution more closely resembles those of radiosonde measurements, which are skewed towards lower depths rather than being symmetric. However, the inferred distributions may be biased due to the vertical resolution of the LIDAR not being able to detect contrails less than 120 m in depth. Therefore, ISSRs less than 120 m in vertical extent are not sampled.

3.2.2 APCEMM-inferred Wind Shear

The HiDepth case results in lower inferred wind shear values, with a mean/median of 0.0057 s^{-1}/0.0053 s^{-1} compared to the 0.0071 s^{-1}/0.0060 s^{-1} of the base case. This is because as contrail depth increases, the wind shear value required to produce a contrail of a given width decreases. Like with the ISSL depth, changing the temperature or EI_{nvPM} does not significantly affect the distribution of APCEMM-inferred wind shear values. This is because temperature and EI_{nvPM} primarily affect the ice physics of the contrail rather than its short-term spatial diffusion.

The mean inferred wind shear values for all cases are within the ranges for measurements of mean wind shear at cruise altitudes in literature, where studies analyzing radiosonde measurements of wind shear [36] [20] have found average cruise altitude wind shear values of 0.005 s^{-1} to 0.01 s^{-1}, depending on the latitude.

3.2.3 APCEMM-inferred RH$_i$

Modifying the temperature, EI$_{nvPM}$, and initial depth parameters all have an effect on the resulting inferred RH$_i$ distribution. The HiTemp case infers a lower mean/median RH$_i$ of 108.5%/105.0% compared to the 110.5%/107.1% of the base case due to more water vapor being required to reach a specified RH$_i$ as temperature increases, resulting in a lower RH$_i$ required to achieve a specified ice growth rate and IOD for the contrail. The LowSoot case shows an over 100% increase in average supersaturation with an increase in the mean/median inferred RH$_i$ to 122.0%/116.9%. This is due to to contrail ice mass and optical depth having a positive correlation with the initial ice crystal number. Therefore, a higher RH$_i$ would be required to achieve the same observed IOD in the LowSoot case. For the HiDepth case, the mean/median inferred RH$_i$ increased to 114.6%/108.1%, possibly due to contrails that are initially deeper having a higher fraction of their particles cut off by extending below the limit of the ISSL, resulting in an effectively lower EI$_{nvPM}$.

Radiosonde measurements of ice supersaturation [37] [38] [39] suggest that median RH$_i$ for ISSLs is between 104 to 110%. All APCEMM cases except LowSoot have their medians within this range, and this aligns with the fact that most in-service aircraft are equipped with engines that on average produce EI$_{nvPM}$ approximately 10^{15} particles per kg fuel [40].

3.2.4 CoCiP-inferred Ambient Parameters

CoCiP infers a lower mean/median ISSL depth of 196 m/209 m compared to the 323 m/266 m as inferred by the APCEMM HiDepth case that best matched the radiosonde observations. In the case of CoCiP, the inferred ISSL depth is an estimate of the minimum ISSL depth required for contrail formation rather than an estimate of the actual ISSL depth. This is because CoCiP does not con-

sider factors involving the vertical profile of the contrail, such as contrails being partially cut off by ice subsaturated regions. If the ISSL depth is high enough for the contrail to persist after the vortex phase, the CoCiP output is not a function of the ISSL depth, provided that the representative altitude of the contrail stays in the ISSL.

In terms of inferred wind shear, CoCiP infers a higher mean/median of 0.0080 s^{-1}/0.0060 s^{-1} than the 0.0071 s^{-1}/0.0060 s^{-1} inferred by the APCEMM base model. This is potentially due to the fact that the depth estimation module in CoCiP has not been calibrated on this sample of contrails. This results in consistent underestimates of the contrail depth, which forces a higher inferred shear to reproduce a contrail of the same width. However, averages for inferred wind shear for all models are within the ranges observed by radiosondes, so no conclusion about whether one estimate is better than the other can be drawn.

CoCiP infers a higher mean RH_i of 131.4% compared to the 110.5% as inferred by the base APCEMM case and the 114.6% as inferred by the HiDepth case. Furthermore, 18/152, or 11.8% of cases reach the upper limit (RH_i = 160%) of the optimization domain. The inferred distribution does not agree with radiosonde measurements of RH_i in ISSRs, which suggest that the distribution should be skewed left with values of RH_i above 130% occurring less frequently than values of RH_i between 100% and 110% [39]. This suggests that the IOD in CoCiP is less sensitive to RH_i than the IOD is in APCEMM, and that there could be sources of error arising from this lower RH_i sensitivity when using CoCiP for contrail modeling.

3.3 Biases in ERA5 Data

Figure 9 compares the distributions of ambient parameters as inferred by APCEMM and CoCiP and as observed in the ERA5 data.
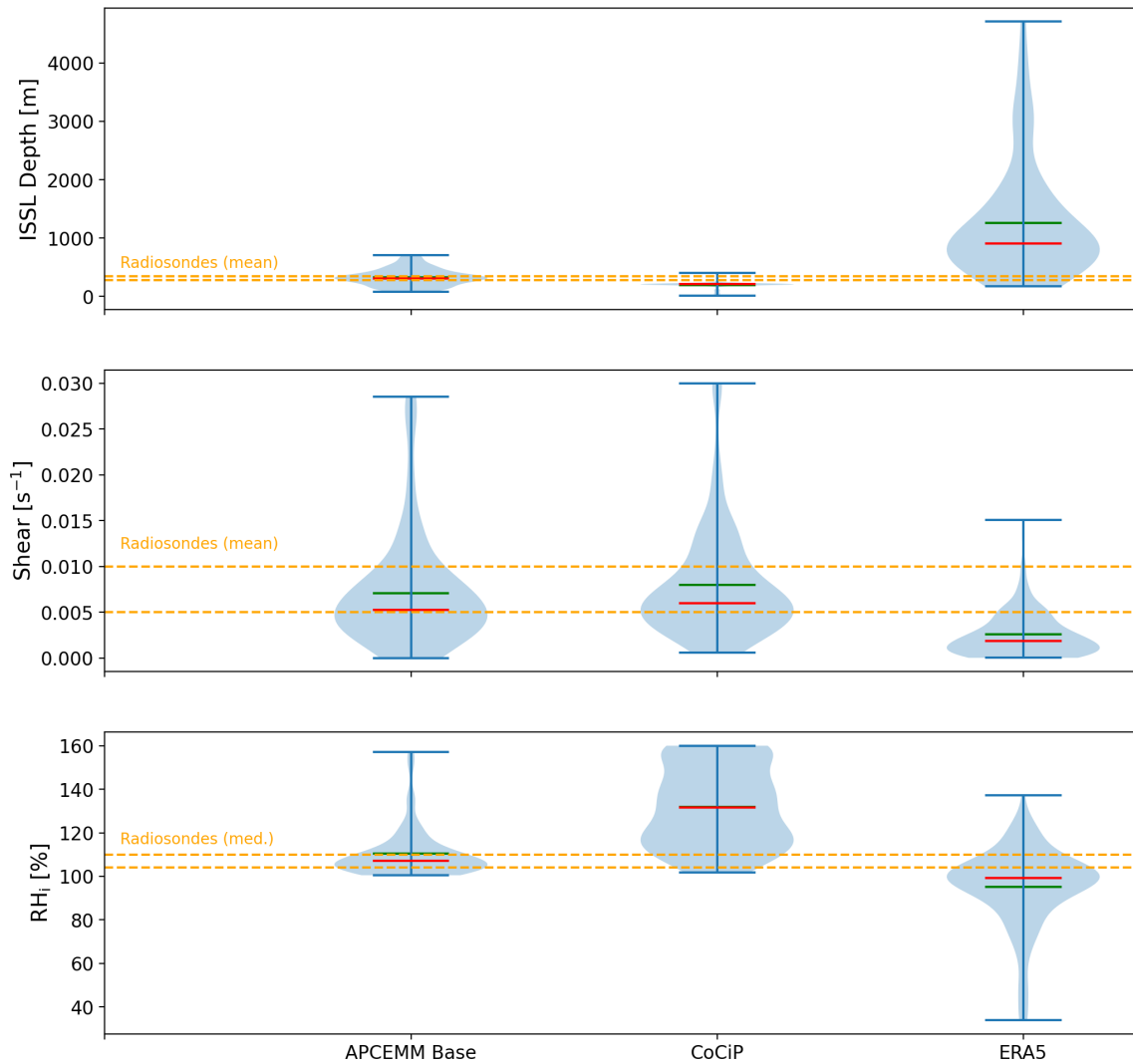
Figure 9: Similar to Figure 8, but compares the distributions of model-inferred parameters to those observed in the ERA5 data. Orange dotted lines show the range of means and medians in radiosonde measurements.

Using ERA5 data as-is overestimates the ISSL depth for the 65 (of 152) cases that form a contrail with a mean of 1262 m compared to the mean of 332 m as inferred by the APCEMM HiDepth model. Some of this disparity can be explained by ERA5's coarse vertical resolution of 1 km when using the most accessible output format. However, since the RH_i profile and ISSL depth is calculated using nearest-neighbor interpolation, this does not explain why the median ISSL depth would be greater

than one half the grid spacing. Radiosonde measurements find that most ISSLs are less than 1 km in total vertical extent [18][37], but the ERA5 data does not agree with the measurements. Another possible factor causing this discrepancy could be the presence of multiple ISSLs at a single geospatial grid point. It is possible that if two ERA5 data points are 1 km apart in altitude and both points are ice supersaturated, they may be in two separate, smaller ISSLs rather than in the same ISSL that would be larger in vertical extent.

ERA5 is known to underestimate the magnitude of the wind shear compared to radiosonde measurements [20], and this is apparent when viewing the distributions of wind shear as seen by ERA5 and as inferred by APCEMM in Figure 9. The mean ERA5-observed wind shear is 0.0025 s^{-1}, while the lowest mean APCEMM-inferred shear is 0.0057 s^{-1}, suggesting a minimum underestimate by 56.1% in the average wind shear – if the APCEMM-inferred estimate is accurate.

The mean RH$_i$ as observed in the ERA5 data is 95.10%, while the mean RH$_i$ inferred by APCEMM-Base is 110.5%. ERA5 is known to underestimate ice supersaturation when it is known that a contrail forms; that is why implementations of CoCiP such as pycontrails allow users to select a humidity scaling module. This difference can be visualized in Figure 9. If cases where the ERA5 RH$_i$ is less than 100% are excluded, the ERA5 mean/median observed RH$_i$ is 108.3%/105.3, which shows agreement with the APCEMM inferences and radiosonde measurements. These results do not imply that ERA5 underestimates RH$_i$ in the general case, only that there are large uncertainties in the humidity data when simulating individual contrails. Agrawal et al. (2022) [19] found that ERA5 reanalysis-driven simulations can overestimate persistent contrail formation by over 100%. Therefore, although ERA5 shows a false negative rate of 57.2% in this study, it does not imply that there should be a general biasing of the humidity data to force the formation of more contrails.

3.4 Quantifying Weather Data and Modeling Error

Figure 10 shows the distribution of signed percent error in contrail depth, width, and IOD when using APCEMM and CoCiP with the cases as described in Table 2.
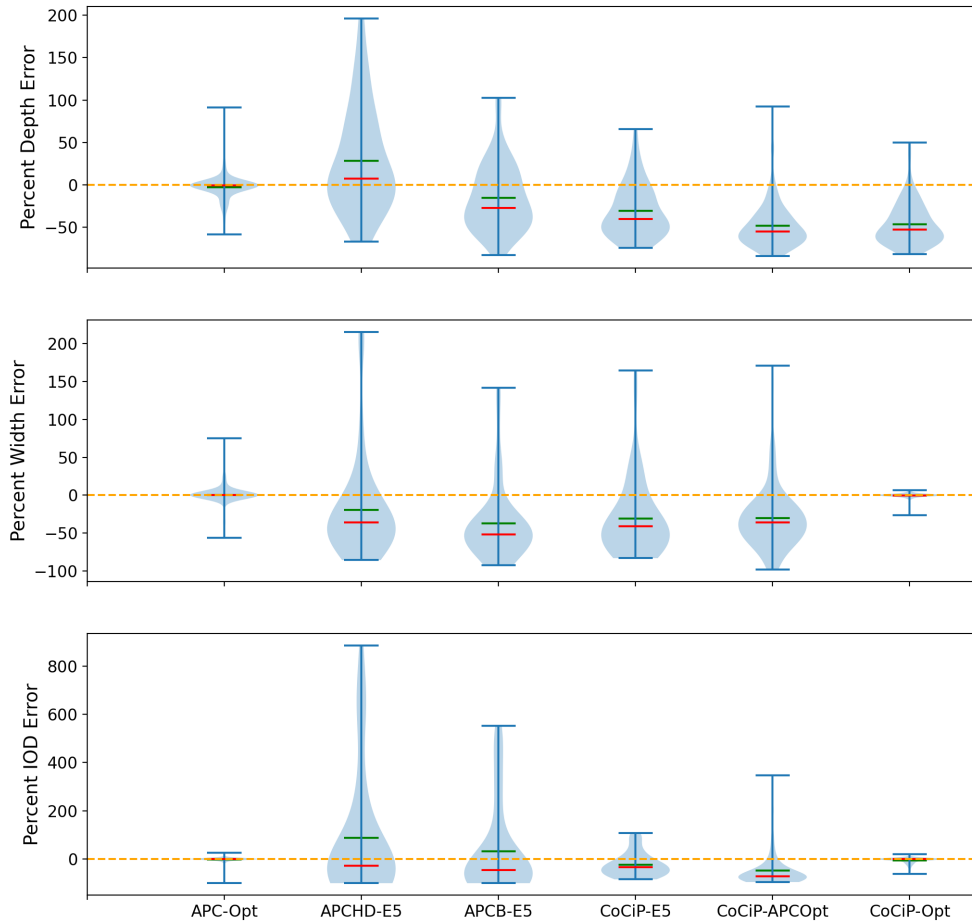
Figure 10: Distributions of signed percent error in contrail width, depth, and IOD for cases listed in Table 2. Green lines indicate the means of the distributions, while the red lines indicate the medians. The ERA5 cases include only the flights where a contrail formed in all three models, while the optimized cases include all flights.

3.4.1 Performance of Ambient Parameter Inference

The "APC-Opt" case, as seen in Figure 10, demonstrates that if allowed to infer the ambient parameters required to form a contrail, the APCEMM-HiDepth model can typically reproduce the

observed contrails to a high degree of accuracy, with a median absolute percent error in depth, width, and IOD of 1.8%, 1.0%, and 0.69% respectively. This combined with the agreement between the radiosonde measurements in literature and the APCEMM-inferred distributions suggests that if the ERA5 data is used as inputs for APCEMM, the resulting errors in depth, width, and IOD are primarily attributable to errors in the ERA5 data rather than APCEMM's simulation of the contrail physics.

The CoCiP-inferred parameters allow the model to reproduce the contrail width and IOD with median absolute errors of 0.82% and 1.05% respectively for the CoCiP-Opt case. However, the inferred parameters do not reproduce the observed depths, with a median 53% error in contrail depth. This implies that CoCiP has sufficient degrees of freedom to adjust the contrail width and IOD based on the wind shear and RH_i, but not to adjust the contrail depth to the ISSL depth.

3.4.2 ERA5 Data Related Errors

The results when using ERA5 rather than the inferred parameters reveal differences in model behavior. For all cases where contrails formed (i.e. not including cases where one model formed a contrail, and the others did not), APCEMM-HiDepth is the most accurate in terms of contrail depth in a median sense, with a median/mean percent depth error of 7.17%/28.39% and a mean absolute error of 47.9%. This is expected, as APCEMM-HiDepth uses the ERA5-optimized depth estimation parameters as derived in Section 3.1. The APCB-E5 case systematically underestimates the contrail depth, with a median / mean percent error of -26.9%/-15.2% and a mean absolute error of 35.3%. This suggests that when using a higher fidelity model such as APCEMM, an absolute percent depth error on the order of 40%, biased towards either underestimation or overestimation depending on the initial depth settings, could be attributed to errors in the ISSL depth.

All cases using the ERA5 data underestimate the width due to the systematic bias in ERA5 towards lower values of wind shear. Even though the APCHD-E5 case typically overestimates contrail depth, it underestimates contrail width with a median/mean percent width error of -36.2%/-19.5%.

The APCB-E5 case underestimates the width more than APCHD-E5 does due to errors from underestimating contrail depth carrying over and resulting in further underestimates in contrail width, with a median/mean error of -52.0/-36.9%. Since one model overestimates and the other underestimates contrail depth, a bound of 20% to 37% can be placed on the average underestimation of contrail width attributable to errors in ERA5 wind data.

Errors in the IOD do not show a consistent sign of bias towards underestimation or overestimation for either APCEMM model, but the magnitudes are larger than errors in depth or width. APCHD-E5 shows a median/mean/absolute mean IOD error of -26.8%/87.8%/164%, and APCB-E5 shows -45.7%/31.9%/124%. This large variance in IOD errors is due to the sensitivity of IOD to RH_i. This strong dependence between IOD and RH_i is supported by LES studies such as Lewellen (2014) [9], where increasing RH_i from 110% to 130% increased the ice surface area, which is correlated with the IOD, by up to an order of magnitude of a contrail of the same age. As the ERA5 RH_i distribution has a mean and median within the range of radiosonde measurements for ISS regions, IOD error is less systematic than wind shear error, but on average greater in magnitude due to the sensitivity of IOD to RH_i. These results suggest that an over 100% average absolute error in IOD when using higher fidelity models such as APCEMM can be attributed to differences between the ERA5-observed and the actual RH_i.

Other factors such as the underestimation of wind shear could contribute to the variance in IOD error, but RH_i uncertainty is the main contributor. A parameter sweep showed that the average IOD increased by no more than 20.1% when increasing the wind shear from 0.0005 s^{-1} to 0.004 s^{-1} assuming an ISSL depth of 500 m and an RH_i of 110%, while increasing RH_i from 110% to 130% assuming an ISSL depth of 500 m and a wind shear of 0.004 s^{-1} resulted in a 232% increase in average IOD.

3.4.3 Errors from CoCiP Modeling Assumptions

When isolating the errors arising from CoCiP's modeling assumptions by using the APCEMM-inferred ambient parameters as inputs, CoCiP systematically underestimates in all three metrics of

43

comparison. The depth, width, and IOD are have median/mean errors of -55.1%/-48.4%, -36.1%/-30.1%, and -71.7%/-47.9% respectively. The IOD mean absolute error is 72.5%.

The depth being systematically underestimated is as expected, since the APCEMM-HiDepth model is calibrated to estimate higher depths based on feedback from LIDAR observations suggesting that CoCiP underestimates initial contrail depth. However, it is unclear whether CoCiP in its current state would necessarily see improvements in its ability to accurately represent the vertical extent of contrails if it were also tuned in favor of higher estimates of initial contrail depth. This is due to its inability to sublimate parts of contrails that have sunk into an ice subsaturated region. This effect is not as apparent in this comparison when the observed cross sections are all estimated to be under 3 hours of age and the gravitational settling has not had time to take effect, but the implications may be more significant when analyzing lifetime contrail behavior.

Like with the depth, CoCiP systematically underestimates the contrail width. This is as expected, since underestimates in contrail depth lead to underestimates in contrail width. This result does not suggest that CoCiP is more or less sensitive to wind shear than APCEMM is.

The source of the IOD errors is likely from CoCiP's low sensitivity to RH_i compared to APCEMM. Although factors such as underestimating contrail depth may contribute to errors in the CoCiP-APCOpt case, the lower sensitivity to RH_i becomes apparent when looking at the CoCiP-E5 IOD error distribution as well the CoCiP-inferred RH_i distribution as seen in Figure 8. The standard deviation of the CoCiP-E5 IOD error distribution is 50.0% compared to the 256% of APCHD-E5 and the 181% of APCB-E5, suggesting that the IOD in APCEMM could be over 3 times more sensitive to RH_i compared to the IOD in CoCiP.

This analysis of modeling versus weather data error suggests that magnitude of errors in contrail depth attributable to CoCiP's modeling assumptions ($\sim$50%) are slightly larger than those attributable to errors in the ERA5 ISSL depth when using APCEMM ($\sim$40%). CoCiP's average underestimate of width ($\sim$30%) is within the range of APCEMM underestimates in width ($\sim$20-

37%) due to ERA5 data bias. Differences between these two error sources appear when analyzing IOD error. CoCiP modeling error is more biased in that CoCiP underestimates IOD by over 70% for more than half the cases compared to the APCEMM models' median IOD errors that are closer to zero. However, the absolute magnitude of the percent error attributable to modeling ($\sim$70%) is less than that shown by APCEMM when using the ERA5 data ($\sim$120-160%). This is likely a result of CoCiP's lower sensitivity to RH_i.

3.5   Energy Forcing and Lifetime Results

Figure 11 shows a comparison between the distributions of contrail lifetime and energy forcing per contrail meter as estimated by APCEMM and CoCiP, both when using the ERA5 data and when relying on the model-inferred ambient conditions. Only the 58/152 cases where the ERA5 data formed a contrail in all 3 models are considered.
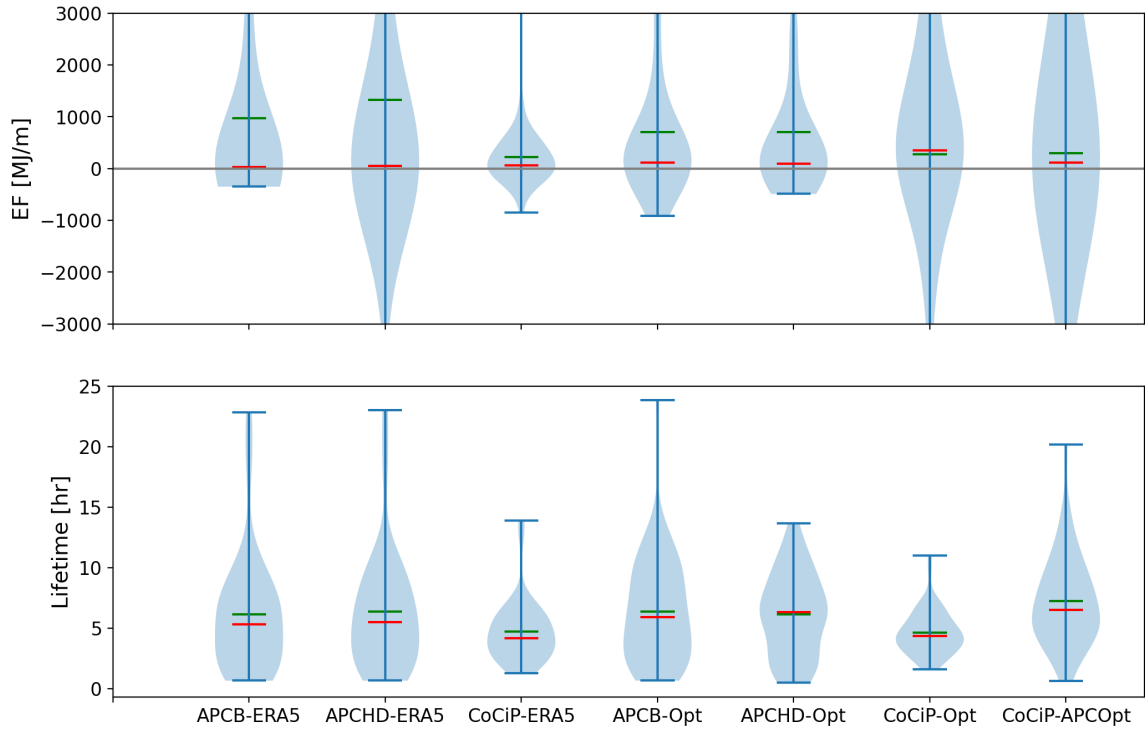
Figure 11: Comparisons of net EF (top) and contrail lifetime (bottom) distributions as simulated by APCEMM and CoCiP using the ERA5 data and with model-inferred parameters. Cases are as described in Table 3. Green lines indicate the means of the distributions, while the red lines indicate the medians. Only cases where the ERA5 data formed a contrail in all models are included. The range of the EF plot is limited to (-3000, 3000) MJ/m to highlight the differences between the distributions.

3.5.1 Using ERA5 Data

When using the ERA5 data, both APCEMM models predict a higher mean energy forcing than CoCiP, with APCEMM-Base/APCEMM-HD predicting an average per-meter EF of 970.0/1322 MJ/m, 4.34/5.92 times the 233.4 MJ/m predicted by CoCiP. However, the median predicted EF is actually smaller than that of CoCiP, with APCEMM-Base/APCEMM-HD predicting a median EF of 22.9/54.0 MJ/m compared to the 59.3 MJ/m predicted by CoCiP. This implies that while the APCEMM models do not necessarily predict a higher EF than CoCiP for the median contrail, there are cases where APCEMM predicts a much higher EF than CoCiP does, skewing the distribution. This is apparent upon examining the standard deviation of the predicted contrail EF, where

APCEMM-Base/APCEMM-HD shows a standard deviation 3.73/5.43 times that of CoCiP.

There a number of potential explanations for these differences. First, APCEMM, when given the ERA5 data, predicts contrails with higher and more varied integrated optical depths due to its higher sensitivity to RH_i compared to CoCiP. IOD and contrail properties correlated with it, such as the ice particle size distribution, are directly linked to the contrail's RF.

Additionally, as seen in Figure 11, the APCEMM models predict longer contrail lifetimes using the ERA5 data compared to CoCiP, with an average predicted lifetime of 6.13 hours with the base model compared to the 4.74 hours predicted by CoCiP, a 29.3% increase. This difference stems from the ways the two models treat the vertical RH_i profile and the mixing of the contrail with the ambient air. CoCiP only tracks the vertical position of the contrail at with one point. Therefore, if RH_i at that singular point is subsaturated, CoCiP will interpret that as the entire contrail being in subsaturated air, even though there may be parts of the contrail still in ice supersaturated air. Moreover, CoCiP assumes that ambient air mixes throughout the contrail cross section every time step. This may result in contrails sublimating quickly after encountering subsaturated air. In APCEMM, where the mixing process is explicitly simulated, the parts of the contrail farthest from the contrail core would sublimate first from the mixing of subsaturated air, slowing overall evaporation. If the contrail is quickly advected back into an ice supersaturated region after a brief encounter with subsaturated air, the contrail core may even survive in cases where CoCiP would have ended the simulation.

The CoCiP-predicted average contrail EF of 223 MJ/m slightly lower than the range of regional averages of 237-402 MJ/m reported in Teoh et al. (2023), where CoCiP was used to quantify global contrail climate impacts. However, the difference is small enough to be explainable by the lower sample size of in this study, given the standard deviation of 592 MJ/m for the CoCiP-predicted EF distribution.

3.5.2   Using Model-inferred Parameters

When using the ambient parameters as inferred by each model, the APCEMM models converge in the EF distribution, with a 0.857%/7.88% difference in the mean/standard deviation. APCEMM predicts a 2.59 times higher EF than CoCiP with its inferred ambient parameters. CoCiP continuing to predict a smaller EF despite inferring higher values of RH_i further suggests a lower sensitivity between RH_i and properties that affect contrail RF, such as optical depth and ice crystal size. The convergence of the APCEMM models suggests that the contrail properties after the age of observation (typically earlier than 2 hours) possibly have a limited sensitivity to small changes in the ISSL depth, wind shear, and RH_i. Ambient parameter inference forces the two APCEMM models to produce the same result at the time of observation, but the results are allowed to diverge after this point in time. Nonetheless, the EF results remain similar for lifetime simulations.

The average contrail lifetime did not differ by more than 4% between using the ERA5 data and the inferred parameters for any model. For the APCEMM models, this could suggest that using the ERA5 data with APCEMM produces contrails of lifetimes statistically similar to cases with a fixed RH_i and ISSL depth, but a larger sample size would be required to support this claim given the systematic differences in the ERA5 and APCEMM-inferred ISSL depth distributions. In the case of CoCiP, the lifetimes did not significantly increase, despite the constant RH_i and ISSL depth removing the potential issue of CoCiP's instant mixing assumptions shortening lifetimes. This leaves a few remaining explanations. CoCiP's higher inferred values of RH_i would lead to higher ice particle growth and lower lifetimes, potentially cancelling out the gain in contrail lifetimes from having a constant RH_i and ISSL depth. Furthermore, CoCiP infers smaller ISSL depths than APCEMM, which would exacerbate the effects of CoCiP not resolving the vertical profile of the contrail.

The results of the CoCiP-APCOpt case suggest that CoCiP is able to reproduce APCEMM's distribution of contrail lifetimes when given identical weather data constant in time, but still predicts an average EF 60% smaller compared to the APCEMM models. The similar lifetimes suggest that the cause of CoCiP's shorter predicted lifetimes for the ERA5 case is primarily due to its mixing assumptions. This also suggests that in addition to the shorter lifetimes with the ERA5 data,

CoCiP's lower sensitivities between RH_i and RF-impacting contrail properties contribute to the model estimating a smaller EF compared to APCEMM.

4 Conclusions

4.1 Summary of Thesis Findings

1. APCEMM is updated through replacing the spectral solver with a finite volume solver, the introduction of the LAGRID algorithm, and modules that simulate the effects of initial contrail aspect ratio, turbulent temperature fluctuations, and vertical advection. A factor of 20 (3) improvement in runtime for a 3 (10) hour contrail simulation is observed with a total runtime of 25.5 (555) seconds on 8 CPU cores. Turbulent fluctuations are found to cause a decrease in the time-dependent ice particle number and mass, consistent with LES results.

2. Distributions of ISSL depth, wind shear, and RH_i inferred by APCEMM show agreement with radiosonde measurements. CoCiP infers an approximately 40% lower average ISSL depth compared to APCEMM and radiosonde measurements due to limitations in its representation of the contrail's vertical profile and an approximately 3 times higher average ice supersaturation due to the lower sensitivity of its optical depth to RH_i.

3. The ERA5 data shows a 3.8 times higher average higher ISSL depth, 56.1% lower average wind shear, and similar average RH_i compared to APCEMM inferences and radiosondes for cases where $RH_i > 100\%$.

4. Biases in the ERA5 wind shear data result in a systematic underestimate of contrail width by 19.5%-36.2% when using APCEMM. The distributions of the depth and IOD errors are more symmetric. Errors in the IOD due to incorrect RH_i data are the largest in magnitude, with an average absolute IOD error of approximately 164% compared to the 47.8% for contrail depth and maximum 36.2% underestimate in contrail width.

5. CoCiP's modeling assumptions are estimated to account for an average signed percent error in contrail depth/width/IOD of -48.4%/-30.1%/-47.9%. Possible causes for these errors include

CoCiP uncalibrated depth estimation parameters, its inability to simulate a partially subsaturated vertical humidity profile, and its low sensitivity to RH_i. However, this lower sensitivity to RH_i is also found to result in smaller average absolute errors in IOD when using the ERA5 data compared to APCEMM.

6. APCEMM is found to produce contrails with a 29.3% longer lifetime and a 4.34-5.92 times higher EF per contrail length compared to CoCiP when using the ERA5 data. This could be due to CoCiP's low sensitivity of IOD to RH_i and its limited representations of the vertical contrail profile and the mixing of the contrail with entrained ambient air. CoCiP produces contrails of similar lifetimes and an average 60% smaller EF compared to APCEMM when using the APCEMM-inferred parameters, suggesting that CoCiP's lower estimate of contrail lifetimes is primarily due to its representation of mixing, and that the lower sensitivity to RH_i leads to lower estimates in contrail EF. Two versions of APCEMM converge in EF results if using their inferred parameters, suggesting that contrail EF results after a certain age may have limited sensitivities to small changes in ambient parameters.

4.2 Recommendations for Future Work

Based on the findings of this thesis, there are a number of paths in which this work can be extended, as described below:

1. **An analysis of uncertainties in contrail properties and RF due to mesoscale turbulence and gravity waves.** In this thesis, we assume a zero turbulent temperature fluctuation due to difficulties in inferring values from the ERA5 weather data. This likely causes a systematic overestimate of contrail RF, lifetime, and IOD. Even if meteorological parameters such as RH_i and wind shear are known at a given point, there is still significant uncertainty due to mesoscale atmospheric turbulence and gravity waves that can cause a decrease on the order of 50% in lifetime integrated optical depth. A follow-up study quantifying the implications of these uncertainties would provide insights into these modeling challenges beyond only the raw weather data and the modeling assumptions.

2. **Continued development of contrail modeling efforts.** One avenue for improving contrail

models is continued work on making existing contrail models represent more physical phenomena that affect the lifetime behavior of a contrail. For instance, it may be interesting to see how CoCiP could better infer the ice supersaturated layer depth if there was a module that tracked the altitudes of the top and bottom of a contrail relative to the RH_i profile, and how that would affect the results. The model's ice physics can potentially be calibrated to improve its representation of optical depth as a function of RH_i. Models can also be developed to account for more processes. Examples would include a heat tracer to account for the timescales required for the contrail to reach the temperature of the ambient air, or a module accounting for stretching of the contrail.

3. **More precise calibration of contrail models.** This thesis attempts to calibrate the initial contrail depth estimation in APCEMM using the LIDAR observations. However, these efforts may be more successful if it is possible to minimize certain uncertainties, such as the ambient meteorological conditions. A possible scenario for this may involve in-situ measurements of ambient meteorological conditions prior to performing test flights, which would put a smaller bound on the ambient conditions. If it is possible to achieve a smaller uncertainty bound in parameters such as the initial depth of a contrail given a set of meteorological conditions, it may also benefit efforts in areas such as correcting the weather data for contrail modeling.

4. **Uncertainty quantification efforts in flight and cross section attribution.** This thesis relies on comparing model results to LIDAR observations attributed to flights and take these observations as the ground truth to compare to. In reality, there is uncertainty associated with flight attribution due to use of the ERA5 wind data, as well as uncertainty on the contrail age, especially for the young contrails in the sample dataset used in this thesis. There is also uncertainty in retrieving the LIDAR ratio and therefore the extinction cross section. Extending this analysis would allow the derivation of an upper limit on the uncertainty attributable to factors other than the model inputs.

5. **An in-depth sensitivity analysis on contrail models.** This thesis showed that APCEMM typically produces contrail with higher EF compared to CoCiP, regardless of whether the input weather data is from ERA5 or ambient parameter inference. A followup study may examine

how much each model reacts to changes in the model inputs and ambient parameters, and how much difference is caused by CoCiP and APCEMM's different representations of contrail ice physics and mixing.

References

[1] D.S. Lee, D.W. Fahey, A. Skowron, M.R. Allen, U. Burkhardt, Q. Chen, S.J. Doherty, S. Freeman, P.M. Forster, J. Fuglestvedt, A. Gettelman, R.R. De León, L.L. Lim, M.T. Lund, R.J. Millar, B. Owen, J.E. Penner, G. Pitari, M.J. Prather, R. Sausen, and L.J. Wilcox. The contribution of global aviation to anthropogenic climate forcing for 2000 to 2018. *Atmospheric Environment*, 244:117834, 2021.

[2] U. Schumann. A contrail cirrus prediction model. *Geoscientific Model Development*, 5(3):543–580, 2012.

[3] T. M. Fritz, S. D. Eastham, R. L. Speth, and S. R. H. Barrett. The role of plume-scale processes in long-term impacts of aircraft emissions. *Atmospheric Chemistry and Physics*, 20(9):5697–5727, 2020.

[4] R. Teoh, U. Schumann, E. Gryspeerdt, M. Shapiro, J. Molloy, G. Koudis, C. Voigt, and M. E. J. Stettler. Aviation contrail climate effects in the north atlantic from 2016 to 2021. *Atmospheric Chemistry and Physics*, 22(16):10919–10935, 2022.

[5] Yixiang Lim, Alessandro Gardi, and Roberto Sabatini. Optimal aircraft trajectories to minimize the radiative impact of contrails and co2. *Energy Procedia*, 110, 04 2017.

[6] pycontrails. https://github.com/contrailcirrus/pycontrails, 2024. Online; accessed 5 May 2024.

[7] S. Unterstrasser and K. Gierens. Numerical simulations of contrail-to-cirrus transition – part 1: An extensive parametric study. *Atmospheric Chemistry and Physics*, 10(4):2017–2036, 2010.

[8] David Gottlieb and Steven A. Orszag. *Numerical Analysis of Spectral Methods*. Society for Industrial and Applied Mathematics, 1977.

[9] D. C. Lewellen, O. Meza, and W. W. Huebsch. Persistent contrails and contrail cirrus. part i: Large-eddy simulations from inception to demise. *Journal of the Atmospheric Sciences*, 71(12):4399 – 4419, 2014.

[10] U. Schumann, R. Baumann, D. Baumgardner, S. T. Bedka, D. P. Duda, V. Freudenthaler, J.-F. Gayet, A. J. Heymsfield, P. Minnis, M. Quante, E. Raschke, H. Schlager, M. Vázquez-Navarro, C. Voigt, and Z. Wang. Properties of individual contrails: a compilation of observations and some comparisons. *Atmospheric Chemistry and Physics*, 17(1):403–438, 2017.

[11] Hans Hersbach, Bill Bell, Paul Berrisford, Shoji Hirahara, András Horányi, Joaquín Muñoz-Sabater, Julien Nicolas, Carole Peubey, Raluca Radu, Dinand Schepers, Adrian Simmons, Cornel Soci, Saleh Abdalla, Xavier Abellan, Gianpaolo Balsamo, Peter Bechtold, Gionata Biavati, Jean Bidlot, Massimo Bonavita, Giovanna De Chiara, Per Dahlgren, Dick Dee, Michail Diamantakis, Rossana Dragani, Johannes Flemming, Richard Forbes, Manuel Fuentes, Alan Geer, Leo Haimberger, Sean Healy, Robin J. Hogan, Elías Hólm, Marta Janisková, Sarah Keeley, Patrick Laloyaux, Philippe Lopez, Cristina Lupu, Gabor Radnoti, Patricia de Rosnay, Iryna Rozum, Freja Vamborg, Sebastien Villaume, and Jean-Noël Thépaut. The era5 global reanalysis. *Quarterly Journal of the Royal Meteorological Society*, 146(730):1999–2049, 2020.

[12] U Schumann. On conditions for contrail formation from aircraft exhausts. 5, Jun 1996.

[13] Roberto Paoli and Karim Shariff. Contrail modeling and simulation. *Annual Review of Fluid Mechanics*, 48(Volume 48, 2016):393–427, 2016.

[14] Ralf Sussmann and Klaus M. Gierens. Lidar and numerical studies on the different evolution of vortex pair and secondary wake in young contrails. *Journal of Geophysical Research: Atmospheres*, 104(D2):2131–2142, 1999.

[15] S. Unterstrasser. Large-eddy simulation study of contrail microphysics and geometry during the vortex phase and consequences on contrail-to-cirrus transition. *Journal of Geophysical Research: Atmospheres*, 119(12):7537–7555, 2014.

[16] B. Kärcher, U. Burkhardt, A. Bier, L. Bock, and I. J. Ford. The microphysical pathway to contrail formation. *Journal of Geophysical Research: Atmospheres*, 120(15):7893–7927, 2015.

[17] Peter Spichtinger and Martin Leschner. Horizontal scales of ice-supersaturated regions. *Tellus B: Chemical and Physical Meteorology*, Jan 2016.

[18] Peter Spichtinger, Klaus Gierens, Ulrich Leiterer, and Horst Dier. Ice supersaturation in the tropopause region over lindenberg, germany. *Meteorologische Zeitschrift*, 12(3):143–156, 06 2003.

[19] Akshat Agarwal, Vincent R Meijer, Sebastian D Eastham, Raymond L Speth, and Steven R H Barrett. Reanalysis-driven simulations may overestimate persistent contrail formation by 100%–250%. *Environmental Research Letters*, 2022.

[20] K. Houchi, A. Stoffelen, G. J. Marseille, and J. De Kloe. Comparison of wind and wind shear climatologies derived from high-resolution radiosondes and the ecmwf model. *Journal of Geophysical Research: Atmospheres*, 115(D22), 2010.

[21] F. Schröder, B. Kärcher, C. Duroure, J. Ström, A. Petzold, J.-F. Gayet, B. Strauss, P. Wendling, and S. Borrmann. On the transition of contrails into cirrus clouds. *Journal of the Atmospheric Sciences*, 57(4):464 – 480, 2000.

[22] C. Voigt, U. Schumann, T. Jurkat, D. Schäuble, H. Schlager, A. Petzold, J.-F. Gayet, M. Krämer, J. Schneider, S. Borrmann, J. Schmale, P. Jessberger, T. Hamburger, M. Lichtenstern, M. Scheibe, C. Gourbeyre, J. Meyer, M. Kübbeler, W. Frey, H. Kalesse, T. Butler, M. G. Lawrence, F. Holzäpfel, F. Arnold, M. Wendisch, A. Döpelheuer, K. Gottschaldt, R. Baumann, M. Zöger, I. Sölch, M. Rautenhaus, and A. Dörnbrack. In-situ observations of young contrails – overview and selected results from the concert campaign. *Atmospheric Chemistry and Physics*, 10(18):9039–9056, 2010.

[23] Christiane Voigt, Ulrich Schumann, Andreas Minikin, Ahmed Abdelmonem, Armin Afchine, Stephan Borrmann, Maxi Boettcher, Bernhard Buchholz, Luca Bugliaro, Anja Costa, Joachim Curtius, Maximilian Dollner, Andreas Dörnbrack, Volker Dreiling, Volker Ebert, Andre Ehrlich, Andreas Fix, Linda Forster, Fabian Frank, Daniel Fütterer, Andreas Giez, Kaspar Graf, Jens-Uwe Grooß, Silke Groß, Katharina Heimerl, Bernd Heinold, Tilman Hüneke, Emma Järvinen, Tina Jurkat, Stefan Kaufmann, Mareike Kenntner, Marcus Klingebiel, Thomas Klimach, Rebecca Kohl, Martina Krämer, Trismono Candra Krisna, Anna Luebke, Bernhard Mayer, Stephan Mertes, Sergej Molleker, Andreas Petzold, Klaus Pfeilsticker, Max Port, Markus Rapp, Philipp Reutter, Christian Rolf, Diana Rose, Daniel Sauer, Andreas Schäfler, Romy Schlage, Martin Schnaiter, Johannes Schneider, Nicole Spelten, Peter Spichtinger, Paul Stock, Adrian Walser, Ralf Weigel, Bernadett Weinzierl, Manfred Wendisch, Frank Werner, Heini Wernli, Martin Wirth, Andreas Zahn, Helmut Ziereis, and Martin Zöger. Ml-cirrus: The airborne experiment on natural cirrus and contrail cirrus with the high-altitude long-range research aircraft halo. *Bulletin of the American Meteorological Society*, 98(2):271 – 288, 2017.

[24] Patrick Minnis, Louis Nguyen, David P. Duda, and Rabindra Palikonda. Spreading of isolated contrails during the 2001 air traffic shutdown. Portland, OR, USA, May 2002. 10th Conference on Aviation, Range, and Aerospace Meteorology.

[25] A. D. Naiman, S. K. Lele, and M. Z. Jacobson. Large eddy simulations of contrail development: Sensitivity to initial and ambient conditions over first twenty minutes. *Journal of Geophysical Research: Atmospheres*, 116(D21), 2011.

[26] S. Unterstrasser. Properties of young contrails – a parametrisation based on large-eddy simulations. *Atmospheric Chemistry and Physics*, 16(4):2059–2082, 2016.

[27] Gilbert Strang. On the construction and comparison of difference schemes. *SIAM Journal on Numerical Analysis*, 5(3):506–517, 1968.

[28] P L Roe. Characteristic-based schemes for the euler equations. *Annual Review of Fluid Mechanics*, 18(Volume 18, 1986):337–365, 1986.

[29] D. M. Winker, J. Pelon, J. A. Coakley, S. A. Ackerman, R. J. Charlson, P. R. Colarco, P. Flamant, Q. Fu, R. M. Hoff, C. Kittaka, T. L. Kubar, H. Le Treut, M. P. Mccormick, G. Mégie, L. Poole, K. Powell, C. Trepte, M. A. Vaughan, and B. A. Wielicki. The calipso mission: A global 3d view of aerosols and clouds. *Bulletin of the American Meteorological Society*, 91(9):1211–1230, 2010.

[30] B. Tan, J. Dellomo, R. E. Wolfe, and A. D. Reth. GOES-16 and GOES-17 ABI INR Assessment. In *AGU Fall Meeting Abstracts*, volume 2018, pages A31L–3070, December 2018.

[31] Vincent Meijer, Luke Kulik, Sebastian Eastham, Florian Allroggen, Raymond Speth, Sertac Karaman, and Steven Barrett. Contrail coverage over the united states before and during the covid-19 pandemic. *Environmental Research Letters*, 17:034039, 03 2022.

[32] Vincent R. Meijer. *Satellite-based Analysis and Forecast Evaluation of Aviation Contrails*. Phd thesis, Massachusetts Institute of Technology, Cambridge, MA, June 2024.

[33] Stuart A. Young and Mark A. Vaughan. The retrieval of profiles of particulate extinction from cloud-aerosol lidar infrared pathfinder satellite observations (calipso) data: Algorithm description. *Journal of Atmospheric and Oceanic Technology*, 26(6):1105 – 1119, 2009.

[34] Jean-Charles Dupont, Martial Haeffelin, Jordi Badosa, Gaelle Clain, Christophe Raux, and Damien Vignelles. Characterization and corrections of relative humidity measurement from meteomodem m10 radiosondes at midlatitude stations. *Journal of Atmospheric and Oceanic Technology*, 37(5):857 – 871, 2020.

[35] G. Rädel and K. P. Shine. Evaluation of the use of radiosonde humidity data to predict the occurrence of persistent contrails. *Quarterly Journal of the Royal Meteorological Society*, 133(627):1413–1423, 2007.

[36] Yehui Zhang, Shaodong Zhang, Chunming Huang, Kaiming Huang, and Yun Gong. The tropopause inversion layer interaction with the inertial gravity wave activities and its latitudinal variability. *Journal of Geophysical Research: Atmospheres*, 124(14):7512–7522, 2019.

[37] Neil Dickson, K Gierens, H Rogers, and R Jones. Vertical spatial scales of ice supersaturation and probability of ice supersaturated layers in low resolution profiles of relative humidity. 01 2009.

[38] Gaby Rädel and Keith P. Shine. Validating ecmwf forecasts for the occurrence of ice super-saturation using visual observations of persistent contrails and radiosonde measurements over england. *Quarterly Journal of the Royal Meteorological Society*, 136(652):1723–1732, 2010.

[39] A. Petzold, P. Neis, M. Rütimann, S. Rohs, F. Berkes, H. G. J. Smit, M. Krämer, N. Spelten, P. Spichtinger, P. Nédélec, and A. Wahner. Ice-supersaturated air masses in the northern mid-latitudes from regular in situ observations by passenger aircraft: vertical distribution, seasonality and tropospheric fingerprint. *Atmospheric Chemistry and Physics*, 20(13):8157–8179, 2020.

[40] Gregory J. Smallwood Theodor Rindlisbacher Frithjof Siegerist Elizabeth A. Black Zhenhong Yu Amewu A. Mensah Donald E. Hagen Richard C. Miake-Lye Kevin A. Thomson Benjamin T. Brem Joel C. Corbin Manuel Abegglen Berko Sierau Philip D. Whitefield Prem Lobo, Lukas Durdina and Jing Wang. Measurement of aircraft engine non-volatile pm emissions: Results of the aviation-particle regulatory instrumentation demonstration experiment (a-pride) 4 campaign. *Aerosol Science and Technology*, 49(7):472–484, 2015.

何でもは知らないわよ。知ってることだけ
ー羽川翼ー

I don't know everything, I just know what I know.
- Tsubasa Hanekawa